Available online at www.sciencedirect.com

ScienceDirect

Geochimica et Cosmochimica Acta 273 (2020) 177–204

Geochimica et Cosmochimica Acta

www.elsevier.com/locate/gca

Controls on the shuttling of manganese over the northwestern Black Sea shelf and its fate in the euxinic deep basin

W.K. Lenstra [a,*], M.J.M. Séguret [a], T. Behrends [a], R.K. Groeneveld [a], M. Hermans [a], R. Witbaard [b], C.P. Slomp [a]

[a] Department of Earth Sciences – Geochemistry, Utrecht University, PO Box 80021, 3508 TA Utrecht, the Netherlands
[b] Department of Estuarine and Delta Systems, NIOZ, Royal Netherlands Institute for Sea Research and Utrecht University, PO Box 140, 4400 AC Yerseke, the Netherlands

Received 18 April 2019; accepted in revised form 16 January 2020; available online 23 January 2020

Abstract

Manganese (Mn) is an essential micronutrient for phytoplankton and its cycling interacts with that of iron (Fe). Continental shelf sediments are a key but poorly quantified source of Mn to marine waters. In this study, we investigate Mn release from shelf sediments, its lateral transport (“shuttling”) in the oxic water column over the northwestern Black Sea shelf and its fate in the adjacent euxinic deep basin. We find a high release of Mn from organic-rich, bioirrigated coastal sediments, but negligible mobilization and release of Mn from sediments in offshore shelf regions, because of a low input of organic matter. Most Mn in the water column is present in dissolved form. We suggest that this dissolved Mn is released from coastal sediments and subsequently transported offshore through physical processes. Surface sediments at open shelf and shelf edge stations are highly enriched in Mn when compared to coastal and deep basin stations. Only part of the surface enrichment can be explained by oxidation of porewater Mn. The remainder of this enrichment is likely the result of oxidative removal of dissolved Mn from the water column and deposition as Mn oxides. Using X-ray spectroscopy we show that Mn in surface sediments in this area predominately consists of Mn(IV) oxides (phyllo- and/or tectomanganates). A key difference between Mn versus Fe shuttling is the form in which the metal is transported: while dissolved Mn dominates in the water column over the shelf, most Fe is present in particulate form. Sediment trap data indicate that the vertical transport of both Mn and Fe through the euxinic water column is correlated and is associated with the sinking flux of biogenic particulate matter following the spring and fall phytoplankton blooms. In the sediments of the euxinic basin, Mn is enriched when compared to a detrital Mn background and its burial correlates with that of Fe. This suggests that Mn could be incorporated in pyrite in the euxinic water column. Our results highlight the critical role of organic matter input as a driver of Mn and Fe shuttling over the Black Sea continental shelf and particulate matter as the carrier of Mn and Fe into the euxinic basin.

Keywords: Manganese; Iron; Benthic release; Lateral transport; GEOTRACES

1. INTRODUCTION

Manganese (Mn) is an essential micronutrient for phytoplankton in the ocean (Raven, 1990; Moore et al., 2013). Continental shelf sediments may act as a key source of dissolved Mn in ocean waters (Charette et al., 2016). Furthermore, sedimentary cycling of Mn can interact with the cycles of other trace metals that can limit the growth of phytoplankton, including iron (Fe; Burdige (1993)). Insight into the dynamics of Mn on continental shelves is therefore

* Corresponding author.
E-mail address: w.k.lenstra@uu.nl (W.K. Lenstra).

https://doi.org/10.1016/j.gca.2020.01.031
0016-7037/

critical for our understanding of the role of metals as nutrients in the ocean.

Release of Mn from sediments and its lateral transport over continental shelves, which is termed "shuttling", is a complex function of a range of factors such as the supply of Mn oxides, input of organic matter, bottom water oxygen concentrations and biological and physical transport processes (Slomp et al., 1997; McManus et al., 2012). Production of dissolved Mn in sediments through reductive dissolution of Mn oxides is driven by the degradation of organic matter, associated sulfide production and the presence of Fe(II) (Postma, 1985; Aller, 1994; Burdige, 2006). This dissolved Mn in the porewater can be present as both Mn(II) and Mn(III) (Madison et al., 2013; Oldham et al., 2019). In sediments overlain by oxic bottom waters part of the dissolved Mn will typically re-oxidize in the surface sediment and can form both Mn(III) and Mn(IV) oxides (Nealson et al., 1988; Burdige, 1993; Luther, 2010). In such settings, some dissolved Mn may also escape the sediment through diffusion. Bioirrigating macrofauna can further contribute to release of dissolved Mn to the overlying water (Thamdrup et al., 1994; Berelson et al., 2003; McManus et al., 2012). When bottom waters are depleted of oxygen, dissolved Mn will generally be released to the overlying water through diffusion only (Balzer, 1982; Sundby et al., 1986; Homoky et al., 2011). Under complete and persistent anoxic or euxinic conditions benthic release of dissolved Mn typically decreases because of the depletion of reducible Mn oxides in the sediment (Slomp et al., 1997; Lenz et al., 2015). Sediments overlain by a permanently anoxic or euxinic water column are therefore noted for a lack of Mn (Calvert and Pedersen, 1993; Brumsack, 2006). However, when sulfide concentrations are high, Mn can become associated with pyrite (Lenz et al., 2014; Hermans et al., 2019), or Mn sulfides can form in sediments in such basins (Suess, 1979; Lepland and Stevens, 1998; Lenz et al., 2015).

Dissolved Mn that escapes from sediments overlain by an oxic water column can precipitate as Mn oxide. However, in the presence of dissolved organic matter, complexation of Mn(III) with organic ligands can also occur (Shiller et al., 2006; Krachler et al., 2015). While Mn oxide particles will typically directly sink and settle at the sediment–water interface, Mn complexes with organic ligands (Mn(III)-L) are generally < 0.02 μm (Oldham et al., 2017), and can remain in solution (Faulkner et al., 1994; Sander and Koschinsky, 2011; Oldham et al., 2017) allowing easy lateral transport (Jeandel et al., 2015). On continental shelves, repeated oxidation, deposition, remobilization and/or resuspension of Mn may occur during such lateral transfer.

While the shuttling of Fe on continental shelves has been studied intensively (e.g. Wijsman et al., 2001; Anderson and Raiswell, 2004; Lyons and Severmann, 2006; Raiswell and Canfield, 2012; Lenstra et al., 2019) that of Mn is not well understood. The oxidation of Mn(II) to Mn(III) and Mn(IV) is mainly bacterially-mediated and is much slower than that of Fe(II) (Stumm and Morgan, 1996; Luther, 2010; Learman et al., 2011, 2013). These factors contribute to differences in the benthic release (Burdige, 1993) and transport of Fe and Mn in oxygenated seawater (Klinkhammer and Hudson, 1986). In a recent modeling study of Mn dynamics in the modern ocean, benthic Mn release was parameterized by directly linking it to that of Fe assuming a constant Fe/Mn ratio of 5 (van Hulten et al., 2017). This model assumption was mainly based on observed Fe/Mn ratios in porewater of North Sea shelf sediments (Slomp et al., 1997). Further improvement of such parameterizations requires quantitative and mechanistic insight in the dynamics of benthic Mn release from shelf sediments, including actual *in-situ* benthic release rates of both Fe and Mn. The Black Sea is well-suited for investigations of metal shuttling, given the evidence for Fe shuttling from the coastal zone to the deep basin (Raiswell and Canfield, 2012; Lenstra et al., 2019). While cycling of Mn around the chemocline of the euxinic basin in the Black Sea has been well studied (e.g. Spencer and Brewer (1971); Tebo, 1991; Dellwig et al., 2010), little is known about the Mn supply from the continental shelf, its ultimate fate in the euxinic deep basin and the interactions with Fe.

In this study, we investigate the dynamics of Mn in the sediment and water column along a water depth transect in the northwestern Black Sea including coastal, open shelf, shelf edge and deep basin sites. We combine porewater and sediment depth profiles, *in-situ* benthic flux measurements and water column analyses of Mn (including suspended matter from *in-situ* pumps and sediment traps), to identify the areas of the shelf where Mn is released from the sediment and to assess how Mn is transported across the shelf. Using data from a parallel study on Fe dynamics (Lenstra et al., 2019), we identify differences between Mn and Fe shuttling over the shelf, and propose mechanisms to explain transport and burial of Mn in the euxinic deep basin. Our results highlight that continental shelf sediments could be a more important source of Mn to ocean waters than previously thought.

2. METHODS

2.1. Study area and sampling

Our study sites are located along a water depth transect on the northwestern Black Sea shelf to the deep basin, with water depths ranging from 27 to 2107 m (Fig. 1; Table 1). We sampled six sites on the continental shelf (stations 6, 7, 8, 9, 13 and 14) and two in the deep euxinic basin (stations 2 and 3; Table 1) during a cruise with *R/V* Pelagia in September 2015. The data set for sediments was extended with results for five stations as sampled in June 2013 by Kraal et al. (2017) (stations 2, 3, 4, 6A and 6B; Fig. A.1; Table A.1).

The northwestern Black Sea shelf covers an area of 70.000 km^2 (Wijsman et al., 1999). The Danube River is a major source of terrestrial organic carbon, nutrients and lithogenic particles to the shelf (Popa, 1993; Panin and Jipa, 2002). The coastal zone is characterized by high rates of organic matter input and degradation, high rates of sediment accumulation and high macrofaunal activity. These all decrease towards the shelf edge (Wijsman et al., 1999; Friedrich et al., 2002; Lenstra et al., 2019). In the deep

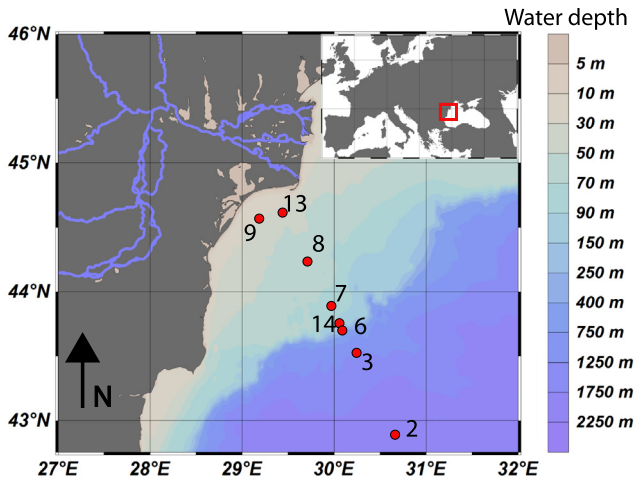

Fig. 1. Locations of the eight stations sampled in the Black Sea in September 2015. Figure drawn using Ocean Data View (Schlitzer, 2015).

Table 1
Coordinates, water depth, bottom water temperature and salinity at the eight stations sampled on the northwestern Black Sea shelf. Unit mbss is meters below sea surface.

Station	Latitude N	Longitude E	Depth mbss	Temperature °C	Salinity
9	44°34.9′	29°11.4′	27	13.3	17.9
13	44°36.5′	29°27.4′	44	9.2	18.1
8	44°14.7′	29°43.4′	65	8.2	18.2
7	43°53.8′	29°58.6′	78	8.5	18.7
14	43°45.9′	30°04.07′	114	8.4	19.5
6	43°42.8′	30°05.1′	130	8.5	20.0
3	43°31.8′	30°15.5′	1100	9	22.3
2	42°4.8′	30°40.7′	2107	9.1	22.3

basin, oxic surface waters are separated from the euxinic waters by a chemocline at 150 m water depth (Arthur and Dean, 1998; Coolen et al., 2009).

The general characteristics of our sites are discussed in detail in Kraal et al. (2017) and Lenstra et al. (2019) (Table 1), but are repeated here briefly for context. Bottom water temperature and salinity at our eight stations ranged from 9 °C to 13.3 °C and 17.9 to 22.3, respectively (Table 1). The lowest temperature and highest salinity were observed at the stations in the deep basin. Organic carbon (C_{org}) contents in the surface sediments (0–0.5 cm), were high at the coastal stations (1.8–2.9 wt%) and in the deep basin (3.8–4.3 wt%) and low at the open shelf and shelf edge stations (0.5–1.3 wt%; Table 2). Bottom water oxygen concentrations were highest at the coastal station 13 (209 μmol L^{-1}) and decreased towards the shelf edge (Table 2). In the deep basin, oxygen was absent and hydrogen sulfide concentrations in the bottom waters increased with water depth (to values up to 418 μmol L^{-1}). Oxygen uptake was highest at the coastal stations 9 and 13, at values of 25.8 and 17.8 mmol m^{-2} d^{-1}, respectively, and decreased offshore. At stations 9 and 13, oxygen penetration in the sediment was 2.25 and 1.65 mm, respectively (Table 2; Fig. A.2).

Water column and sediment samples were collected at eight and six stations, respectively. Depth profiles of conductivity, temperature, density and dissolved oxygen in the water column were obtained with a CTD profiler equipped with an oxygen sensor (SBE43) on a rectangular titanium frame. Water samples were collected using 24 ultra-trace metal clean PVDF samplers attached to the same frame (Rijkenberg et al., 2015), deployed with a Kevlar hydrowire (De Baar et al., 2008; Rijkenberg et al., 2014), except for the coastal stations 9 and 13 that were sampled with a conventional CTD. Sediment cores were collected with an Oktopus multicorer (inner diameter: 10 cm) using polycarbonate tubes of 60 cm length. Only sediments with >20 cm of overlying water and an intact sediment surface were processed further. At all stations, two bottom water samples were taken directly after core retrieval.

At each station, one sediment core was sliced into depth intervals of 0.5 to 3 cm under a nitrogen atmosphere at bottom water temperature (Table 1). Each slice was divided over a pre-weighed glass vial and a 50 mL centrifuge tube. The glass vials were stored under a nitrogen atmosphere at −20 °C for solid phase analyses onshore. The 50 mL centrifuge tubes were centrifuged on board at 4500 rpm for 25 min to extract porewater. Porewater was filtered under

Table 2
Key station characteristics: organic carbon content in the surface sediment (0–0.5 cm), oxygen (O_2) and H_2S concentrations in the bottom water, *in-situ* O_2 uptake as determined with chamber incubations, O_2 penetration depth in the sediment (mm) from microprofiles (Fig. A.2), calculated diffusive flux of O_2, and macrofaunal density (individuals m^{-2}). n.a.= not available. Data presented in this table, except for stations 3 and 2, were previously published in Lenstra et al. (2019) and are repeated here for context.

Station	Organic C wt%	O_2, H_2S Bottom water μmol L^{-1}	O_2 uptake mmol m^{-2} d^{-1}	O_2 diffusive flux mmol m^{-2} d^{-1}	O_2 penetration depth mm	Macrofaunal density ind m^{-2}
9 (coast)	1.8	92, 0	25.8 ± 1.77	13.0	2.25	6179 ± 2051
13 (coast)	2.9	209, 0	17.8 ± 2.8	9.4	1.65	8749 ± 967
8 (open shelf)	0.8	197, 0	8.1 ± 3.4	n.a.	n.a.	5370 ± 3249
7 (open shelf)	0.5	155, 0	3.7 ± 1.4	n.a.	n.a.	4351 ± 2208
14 (shelf edge)	1.3	93, 0	1.6 ± 0.1	n.a.	n.a.	1898 ± 904
6 (shelf edge)	0.9	27, 0	0.4 ± 0.02	n.a.	n.a.	394 ± 199
3 (deep basin)	4.3	0, 381	n.a.	n.a.	n.a.	n.a.
2 (deep basin)	3.8	0, 418	n.a.	n.a.	n.a.	n.a.

a nitrogen atmosphere through 0.45 μm pore size filters and subsampled for Mn and alkalinity. *In-situ* benthic flux measurements were carried out with an Albex lander (Witbaard et al., 2000) at all stations except for stations 3 and 2.

Four sediment traps (Technicap PPS5; surface area of 1.39 m^2) with 24 polypropylene bottles (250 mL) were deployed in September 2015 at station 2 at water depths of 214, 448, 932 and 1716 m. Before deployment all trap bottles were filled with anoxic water as obtained with the ultraclean CTD at the corresponding water depths. During the deployment, each bottle collected particulate material for 15 days from 10 September 2015 until 4 September 2016. All sediment traps were recovered during a cruise with *R/V* Pelagia in March 2017.

2.2. Water column analyses

Unfiltered samples for total dissolvable Mn (henceforth termed TdMn) were taken from the PVDF samplers using acid-washed LDPE tubing. Samples for dissolved Mn (colloidal and aqueous Mn) were obtained using a 0.2 μm Sartobran 300 cartridge (Sartorius), after pre-filtration with 0.5 L of ambient seawater. In all cases, nitrogen pressure was applied at the top of the sampler and the samples were collected in acid-washed 60 mL LDPE bottles (Nalgene), filled to the shoulder of the bottle. Samples were acidified to pH 1.8 by adding 120 μL of distilled 10 M HCl to 60 mL of sample. The acidification of samples may lead to an underestimation of total dissolvable and dissolved Mn concentrations due to precipitation of humic substances upon acidification (Oldham et al., 2017). Samples were stored at 4 °C until analysis.

The concentration of Mn was determined by Inductively Coupled Plasma Mass Spectrometry (ICP-MS) after preconcentration with a SC-DX SeaFAST S2 (Elemental Scientific). Acidified samples (pH 2) were buffered online with a pre-cleaned buffer solution (4.8 M glacial acetic acid 99.7% (Baseline, Seastar) and 4.1 M ammonium hydroxide 29% (Baseline, Seastar), pH 6) and loaded onto the preconcentration column for 20 s (Lagerström et al., 2013). Samples were measured either with an ICP-MS X-series 2 (Thermo Scientific) or a Nexion ICP-MS (Perkin Elmer). When using the X-series ICP-MS, seasalts were rinsed from the preconcentration column using de-ionized water and the analyte was eluted into a 1 mL cuvette with 2 M HNO_3, spiked with 2 ppb Indium (internal standard). When using the Nexion ICP-MS instrument the analyte was injected directly into the instrument and measured online. On the X-series, the limit of detection (LoD) for Mn was 0.138 ± 0.080 nmol L^{-1} (n = 8). On the Nexion, the LoD was 0.0225 ± 0.0007 (n = 6). The value of the blank was typically below the limit of detection. SLEW-3 (Estuarine water reference material for trace metals; National Research Council Canada) was used as a reference material. For each ICP-MS analysis, the results of 30 readings were averaged. We measured an average value of 1.63 ± 0.12 μg kg^{-1} (n = 32), which is consistent with the reference value of 1.59 ± 0.22 μg kg^{-1}. The overall recovery was 102.4 ± 10.6%.

At station 2 water column samples for analysis of hydrogen sulfide (H_2S: sum of H_2S, HS^- and S^{2-}), dissolved inorganic carbon (DIC) and silicic acid (Si) were filtered over 0.2 μm acrodisc filters and directly analyzed on board on a QuAAtro (SEAL Analytical, Germany) auto analyzer. Samples for H_2S were analyzed using the methylene blue method according to Grasshoff et al. (2009). Samples for DIC were acidified online after oxidation with H_2O_2 and analyzed using the alkaline phenolphthalein method according to Stoll et al. (2001). Samples for Si were measured using the molybdate-blue method according to Strickland and Parsons (1972).

Suspended matter was collected through *in-situ* pumping for 1-4 h at 4 water depths per station using four McLane pumps (3x WTS-LV, 1x WTS-LV Dual Filter). After retrieval of the pumps, water around the filters (Supor, 0.8 μm, 142 mm diameter) was removed by vacuum pumping and the filters were placed in petri-dishes, sealed in plastic bags and stored at −20 °C. Manganese in suspended matter was determined on a quarter of every filter in a 4-step sequential extraction procedure (Table A.2). This extraction procedure is specific for a range of Fe phases (Poulton and Canfield, 2005; Claff et al., 2010; Raiswell et al., 2010), but has not been calibrated for Mn. However, the Mn minerals that are dissolved are expected to decrease in reactivity from step 1 to 4, as is known for Fe (Table A.2). After extraction, all solutions were filtered through 0.45 μm pore

size nylon filters. The concentration of Mn in the extraction solutions were determined by Inductively Coupled Plasma Optical Emission Spectroscopy (ICP-OES; Spectro Arcos; LoD: 0.003 μmol L^{-1}). The sum of all Mn phases extracted in the four steps was assumed to represent reactive Mn (i.e. Mn oxides and Mn carbonates; Sulu-Gambari et al. (2016)).

2.3. Pore water analyses and in-situ benthic fluxes

Samples for dissolved Mn were acidified with 10 μL 35% suprapur HCl per mL of sample. Dissolved Mn, likely present as both Mn(II) and Mn(III) (Madison et al., 2013; Oldham et al., 2019), was analyzed by ICP-OES (LoD: 0.003 μmol L^{-1}). Alkalinity was determined by titrating 1 mL of untreated sub-sample with 0.01 M HCl.

Diffusive fluxes of dissolved Mn across the sediment–water interface (J in mmol m^{-2} d^{-1}) were calculated using Fick's first law of diffusion taking into account porosity, ambient salinity, pressure and temperature at each site using the R package CRAN: marelac (Soetaert et al., 2010), which implements the constitutive relations listed in (Boudreau, 1997).

Benthic fluxes of TdMn were determined *in-situ* with a benthic lander, equipped with three chambers made of the inert delrin plastic, each with a surface area of 144 cm^2 and a water volume between 1.3 and 1.8 L (Table S.1-S.6; Witbaard et al. (2000)). A detailed description of the benthic lander and samples analysis is given in Section A.1.

2.4. Solid phase analyses

All sediments were freeze-dried and the porosity was determined from the weight loss upon freeze drying. Freeze-dried sediments were ground in an agate mortar. To determine the total elemental concentrations, sediment was digested in mixed acid (HNO_3, $HClO_4$ and HF) as described by Lenstra et al. (2019). The final solutions were analyzed for total Mn with ICP-OES (Lenstra et al., 2019). The average analytical uncertainty based on duplicates was 4.5% for Mn. Total Fe, aluminum (Al), sulfur (S) and C_{org} contents were previously published in Lenstra et al. (2019) and are repeated here for context. Solid phase concentrations of Mn and Fe normalized to Al are reported in units of wt% $wt\%^{-1}$.

2.5. X-ray spectroscopy

X-ray absorption spectroscopy (XAS) was used to analyze sediments for their Mn mineralogy at beam-line BM26 (DUBBLE) at the ESRF, Grenoble, France (Borsboom et al., 1998; Nikitenko et al., 2008). XAS spectra were collected at the Mn K-edge in the energy range of ca. 6.3–7.1 keV. A detailed description of the energy calibration and data collection is given in Sections A.2 and A.3. Freeze-dried, ground and homogenized surface sediment (0–0.5 cm) from stations 8, 7, 14 and 6A was pressed into pellets in a nitrogen-filled glove bag at the beamline. Each pellet was wrapped in Kapton foil to prevent oxidation during analysis in transmission mode at room temperature. Both X-ray Absorption Near Edge Structure (XANES) and Extended X-ray Absorption Fine Structure (EXAFS) spectra were obtained. The ATHENA software package (Ravel and Newville, 2005) was used to remove the background and for normalization and linear combination fitting (LCF) of spectra. Linear combination fitting allows spectra for samples to be reproduced by combinations of spectra of mineral standards, containing various Mn oxides, sulfides, carbonates, phosphates and silicates (Fig. A.3; Table A.3). For such LCF, we used normalized XANES spectra for the energy range 6530–6700 eV and the k^3 weighted EXAFS spectra in the range 2–11 Å. Due to the low Mn content, XAS spectra for sediments from stations 8 and 7 were of too low quality for analysis. Therefore, only the results for stations 14 and 6A are presented.

2.6. Sediment trap analyses

After retrieval of the four sediment traps, all trap bottles were immediately closed and transferred to a laboratory maintained at *in-situ* temperature. The bottles were stored under a nitrogen atmosphere at 4 °C until further analysis.

Sampling of the material collected in the trap bottles was performed in an argon filled glovebox. Samples were homogenized by gently mixing the contents and then split into equal 3 portions using nitrogen pressure. The exact amount of sample was determined by weighing. One portion was centrifuged at 2800 rpm for 6 min and the supernatant was sampled and filtered over 0.45 μm and divided into two fractions: (1) 5 mL was acidified with 50 μL 35% suprapur HCl and analyzed for dissolved Fe, Mn, Ca and Si by ICP-OES and (2) 2 mL was transferred into a 2 mL airtight glass vial for analysis of DIC using an AS-C3 analyzer (Apollo SciTech), consisting of an acidification and purging unit in combination with a LICOR-7000 CO_2/H_2O Gas Analyzer.

The solid phase was freeze-dried and the total particle flux was determined based on the dry weight of the sample upon freeze-drying and the time that each sample bottle was open (15 days). Subsequently, the material was ground in an agate mortar. Total elemental concentrations of Fe, Mn and Ca were determined as described for sediment samples above. The total Ca concentration was used to calculate the $CaCO_3$ content of the sample. A second subsample of ca. 300 mg was decalcified with 2 wash steps of 1 M HCl (Van Santvoort et al., 2002) and subsequently dried, powdered and analyzed for carbon (C) using an elemental analyser (Fisons Instruments model NA 1500 NCS). Organic C contents were determined after correction for the weight loss following decalcification. A third subsample of ca. 30 mg was subjected to a biogenic silica (SiO_2) extraction procedure following DeMaster (1981). The sample was mixed with 40 mL 0.1 M Na_2CO_3 solution and Si was extracted for 5 h in a continuously shaking water bath heated to exactly 85 °C. After 1, 2, 3 and 5 h a 0.5 mL aliquot was removed from the solution and neutralized with 4.5 mL of 0.021 M HCl. Silica in all samples was measured spectrophotometrically using the molybdate-blue method (Strickland and Parsons, 1972). Concentrations of biogenic silica were determined by fitting a linear regression line to

the concentration change of Si during extraction (DeMaster, 1981). All solid phase analyses were corrected for salt content. Downward fluxes (in μmol m^{-2} d^{-1} or mg m^{-2} d^{-1}) were calculated as follows:

$$\text{Downward flux} = C * \text{sample mass}/(t * \text{surface}_{\text{sed.trap}}) \quad (1)$$

where sample mass is total mass of freeze dried sample in units of g, t is the duration of sample collection in days, $\text{surface}_{\text{sed.trap}}$ is the area of the sediment trap in m^2 and C is the concentration in μmol g^{-1} or mg g^{-1}. The concentrations (i.e. C) were corrected for decomposition, dissolution or precipitation of the solid phase by comparing concentrations of dissolved Fe, Mn, Si and DIC in the sediment traps with water column concentrations at station 2 at corresponding water depths (Supplementary material; dissolved Fe was taken from Dijkstra et al. (2018)). The correction for Ca was applied by calculating the Ca concentration in seawater based on the salinity (Table 1; Pilson (2012)). The difference between the dissolved concentration in the sediment trap and the water column was added to the solid phase concentration. Organic carbon contents were corrected for the change in DIC concentration in each trap bottle. Concentrations of total particle flux, SiO_2 and $CaCO_3$, C_{org} and Fe_{tot} before and after correction were largely similar (Fig. A.4). For Mn, the correction led to a lowering of Mn fluxes, but this did not change the overall trend.

Two freeze-dried subsamples of material from the sediment trap from 214 meter water depth collected in October and April, which were periods with the highest downward particle flux, were additionally analyzed for Fe and Mn content by μXRF. Aliquots were mounted on double-sided carbon tape and elemental maps (0.8 by 0.4 cm) were collected using a Desktop EDAX Orbis μXRF analyzer (Rh tube at 30 kV, 500 μA, no filter, 300 ms dwell time, poly-capillary lens providing a 30 μm spot size).

3. RESULTS

3.1. Water column Mn

At all six shelf stations, concentrations of dissolved Mn and TdMn were elevated close to the sediment water interface and ranged between 4–694 and 21–911 nmol L^{-1}, respectively (Fig. 2A). Concentrations of Mn were relatively low in the remainder of the water column, especially at the open shelf and shelf edge stations (typically below 10 nmol L^{-1}). A distinct offshore decline in both TdMn and dissolved Mn near the sediment surface was observed (e.g. for TdMn, from up to 911 nmol L^{-1} at station 9 to ca. 20 nmol L^{-1} at station 14), after which TdMn concentrations increased again at station 6 (to ca. 80 nmol L^{-1}). A similar offshore decline in TdMn and increase at station 6 was observed in the bottom water samples of the lander incubations (Table S.1-S.6). At the coastal and open shelf stations, dissolved Mn accounted for 85 and 96% of TdMn, in the lowest water column sample. At the shelf edge stations, in contrast, the contribution of dissolved Mn was at most 13%. At the deep basin stations, concentrations of dissolved Mn reached a maximum in the chemocline and decreased again at greater depth. The contribution of particulate Mn in and around the chemocline was relatively small.

3.2. Benthic exchange and porewater Mn

In-situ benthic release of TdMn was highest at the coastal stations 9 and 13 (0.47 and 0.3 mmol m^{-2} d^{-1}, respectively; Fig. 2B; Table 3). At the open shelf and shelf edge stations, fluxes were below 0.05 mmol m^{-2} d^{-1}. *In-situ* fluxes were comparable in range to calculated diffusive fluxes, except at station 13 where the calculated diffusive flux was ca. 3-fold higher (Table 3).

Concentrations of dissolved Mn in the porewater were elevated close to the sediment–water interface (0–2 cm) and subsequently decreased with depth at the coastal and open shelf stations (Fig. 2C). Maximum concentrations of dissolved Mn in the porewaters decreased from the coast towards the deep basin (from 74 to 20 μmol L^{-1}). In the deep basin, porewater concentrations of dissolved Mn were ca. 4 μmol L^{-1}, did not change with depth and were similar to Mn concentrations in the lower part of the water column.

3.3. Suspended matter and sediment Mn

Manganese concentrations in suspended matter at the six shelf stations as determined with the sequential extraction (Table A.2) were highest close to the sediment–water interface (up to 205 nmol L^{-1}; Fig. 3; Table A.4). Maximum concentrations of Mn in suspended matter throughout the water column decreased from the coast (205 nmol L^{-1}) towards the open shelf (5.5 nmol L^{-1}) and increased again at the shelf edge (27.7 nmol L^{-1}). Ascorbate extractable Mn was typically the dominant fraction of Mn in the suspended matter, accounting for on average 44% of the Mn (Fig. 3C), with the remainder being extracted by HCl ($Mn_{ox} + Mn_{carb}$), CDB and oxalate (Mn_{ox2}).

Total Mn in the sediment at the shelf stations was typically highest close to the sediment–water interface, especially at stations 7, 14 and 6, where Mn contents were 232, 574 and 230 μmol g^{-1}, respectively (Fig. 4). The latter stations also had the highest total Mn contents below 5 cm in the sediment with values of 14 to 38 μmol g^{-1} compared to less than 10 μmol g^{-1} at stations 9, 13 and 8. In the deep basin, surface sediments were not enriched and Mn contents varied around ca. 7 μmol g^{-1}. Depth profiles of Mn/Al and Fe/Al generally show similar trends to those of total Mn at all stations (Fig. 4). Highest Mn/Al and Fe/Al ratios were observed at the sediment–water interface at the shelf edge station 14, with values of ca. 4 and 2, respectively.

Average Mn/Al and Fe/Al for the 0–2 and 2–15 cm depth intervals in the sediment show similar offshore trends, with ratios increasing from the coast towards the shelf edge (maximum Fe/Al: 1.2 and Mn/Al: 1.3; Fig. 5A and B; Table 4). The ratios subsequently decrease towards the

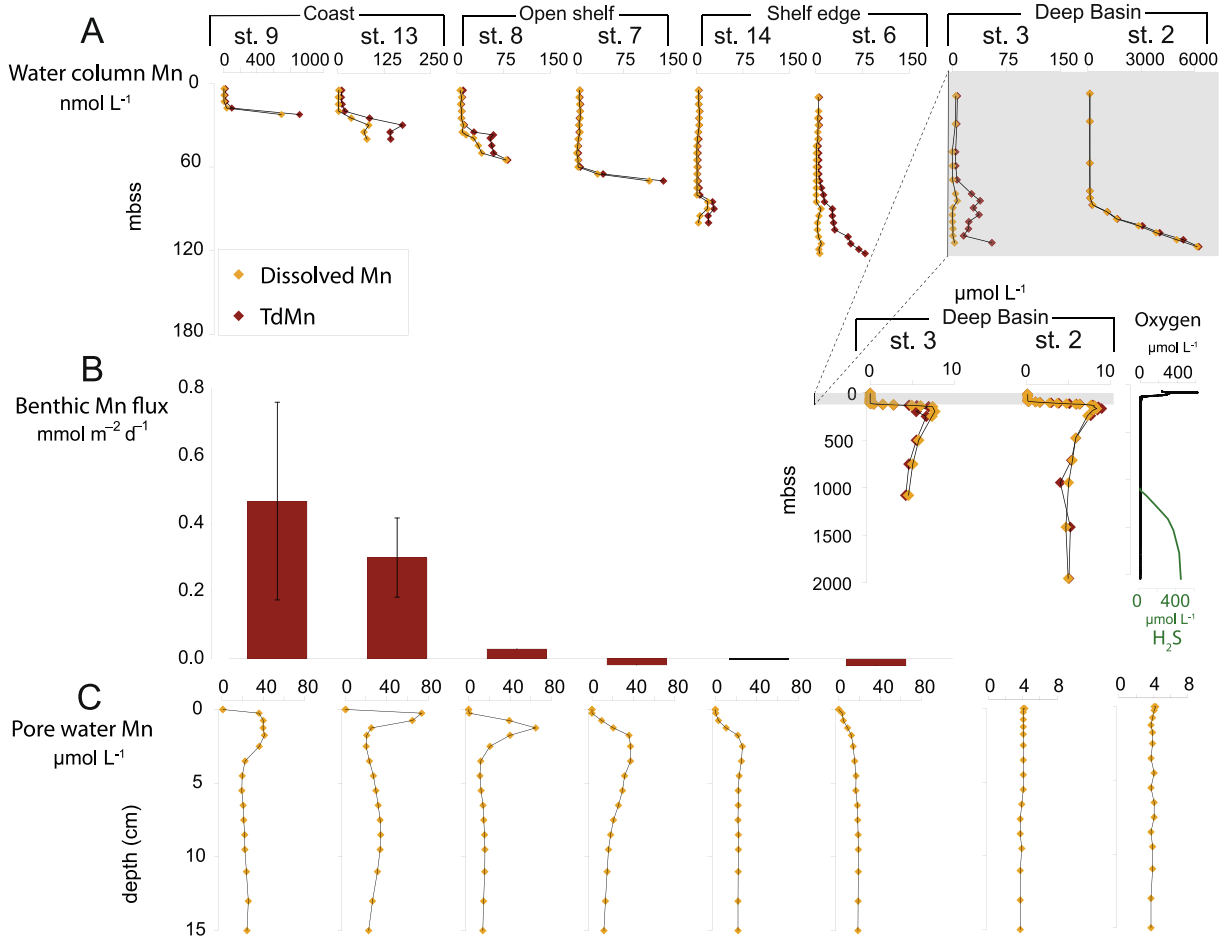

Fig. 2. (A): Water column profiles of TdMn and dissolved Mn (nmol L^{-1}) for eight stations and oxygen and H_2S for station 2; (B): benthic Mn fluxes (mmol m^{-2} d^{-1}) and (C): porewater profiles of Mn (μmol L^{-1}) at our six stations on the northwestern Black Sea shelf and two stations in the deep basin. Porewater data for station 3 and 2 are from Kraal et al. (2017).

Table 3
In-situ measured and calculated diffusive benthic fluxes of Mn. *In-situ* fluxes are averages for three chambers for stations 9 and 13 and values for one chamber for stations 8, 7, 14 and 6. No lander deployment was carried out at station 2. n.a.: not available.

Station	*In-situ* Mn flux mmol m^{-2} d^{-1}	Calculated Mn diffusive flux mmol m^{-2} d^{-1}
9	0.47 ± 0.24	0.5
13	0.3 ± 0.1	1.06
8	0.03	0.006
7	−0.02	0.04
14	0	0.004
6	−0.02	0.037
2	n.a.	0

chemocline and increase again in the euxinic deep basin. The sediment Fe/Mn ratio was highest at the coastal stations and decreased towards the shelf edge (72–0.9; Fig. 5C). In the euxinic deep basin the Fe/Mn ratio was lower than at the coastal stations and decreased further with water depth. In the deep basin Mn/Al strongly correlates with Fe/Al (R^2=0.81; Fig. 6A; depth interval 0–26 cm). Fe/Al and Mn/Al does not strongly correlate with $CaCO_3$ at these stations (Fig. 6B and C).

3.4. X-ray spectroscopy of sediment

The XANES spectra for sediments from stations 14 and 6A (Fig. 7) have a maximum around 6561 eV, which is close to the white line of Mn(IV) (6562; Tebo et al. (2004, 2011)). The spectral shoulder at lower energies indicates that additionally Mn with lower oxidation states was present. The best reproduction of the XANES spectra using LCF with three reference spectra was obtained with birnessite, hausmannite, and rhodochrosite. This indicates that about two third of the Mn in the sediments was present in the form of Mn(IV) accompanied with Mn(II) and possibly some minor amounts of Mn(III). The same combination of reference spectra also gave the best reproduction of the EXAFS spectra but the exact identification of the Mn mineralogy is limited due to the restricted length of the EXAFS spectra.

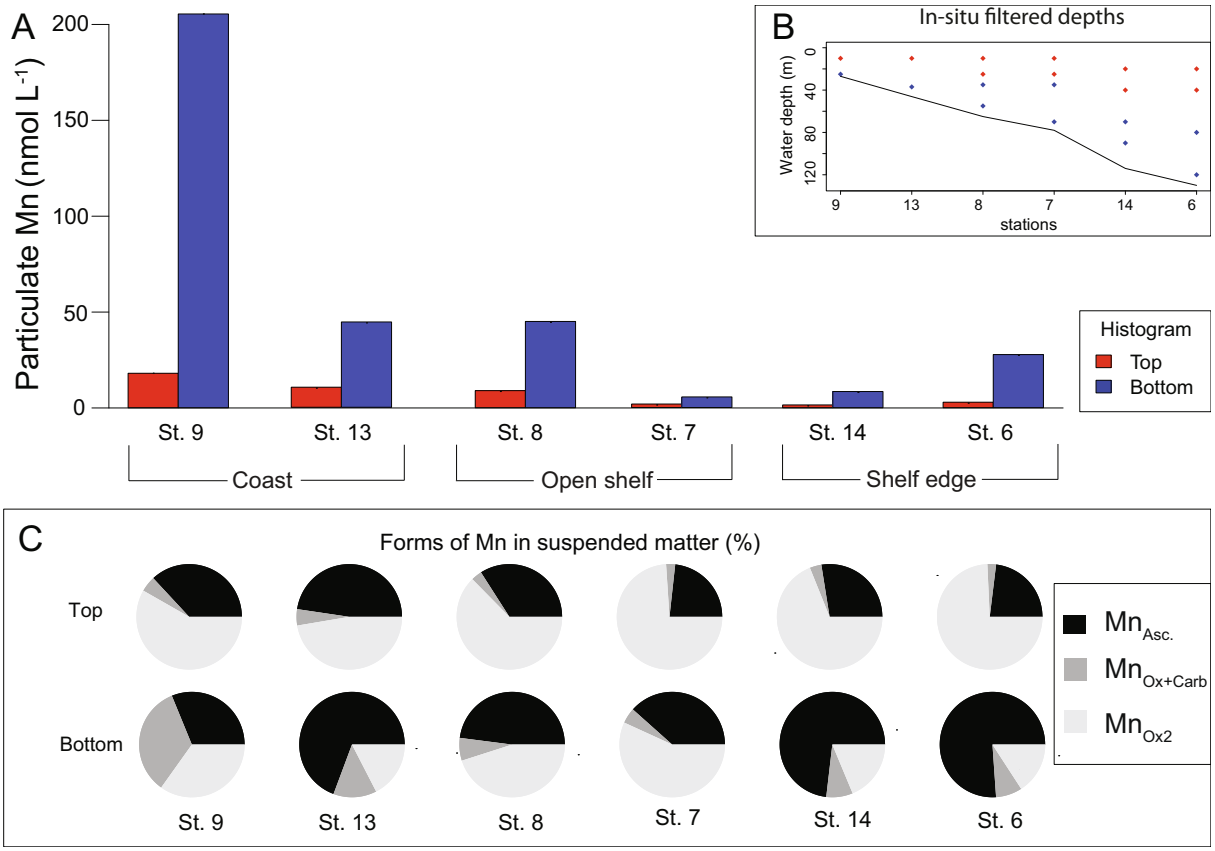

Fig. 3. Mn in suspended matter at six stations on the northwestern Black Sea shelf. (A): Particulate Mn refers to the sum of all Mn fractions upon sequential Mn extraction as calculated for the upper (top) and lower (bottom) part of the water column; (B): water depths at which samples were collected; colors indicate separation into top and bottom. The black line indicates the sediment water interface; (C): forms of Mn in suspended matter (%). Extracted Mn of step 3 and 4 were combined as Mn_{ox2}. Data for individual filters are given in Table A.4. (For interpretation of the references to colour in this figure legend, the reader is referred to the web version of this article.)

The analyzed part of the EXAFS spectra from the sediment is similar to that of the birnessite standard. However, this spectral pattern is found in a variety of phyllo- and tectomanganates (Santelli et al., 2011) and can be ascribed to the resonance features of layers of edge-sharing MnO_6 octahedra.

EXAFS spectra extending to higher k values would be required to distinguish between various phyllo- and tectomanganates containing MnO_2 sheets (Santelli et al., 2011). Diffraction peaks perturbed the EXAFS spectra from station 14 beyond 8 $Å^{-1}$. For station 6A, which had the highest Mn concentrations, LCF was possible in the 2–11 $Å^{-1}$ range and gave similar results as the 2–8 $Å^{-1}$ range (Fig. A.5; Table A.5). Rhodochrosite is consistently included in the best 10 combinations of the combinatorics fitting. The contribution of the rhodochrosite spectrum to the fit accounts for most of the difference between the spectra of the samples and birnessite in the k range of 2.5–4.5 $Å^{-1}$ (Fig. A.3). The presence of hausmannite or Mn(III) oxides is not well constrained based on the linear combination fitting. In summary, the sediments contain Mn(IV) in the form of phyllomanganates and/or tectomanganates (about 60–70% of all Mn in the samples) with some rhodochrosite and possibly other Mn(II) or Mn(III) containing oxides (Fig. 7).

3.5. Sediment trap fluxes

Temporal trends in the flux of particles and Fe and Mn at station 2 between September 2015 and 2016 were similar (Figs. 8A–C). Relatively high rates of downward transport were observed from September to December and April to May, i.e. in autumn and spring. Particle fluxes mainly consisted of biogenic material (i.e. C_{org}, SiO_2 and $CaCO_3$) during these two periods, with a maximum of 70 mg m^{-2} d^{-1} in October. Fluxes of Fe and Mn were also at a maximum in October (at 16.2 and 0.21 μmol m^{-2} d^{-1}, respectively).

No distinct difference in downward Fe and Mn transport between the four sampled depths was observed at times of high flux. However, between May and September, when fluxes were low, downward transport of Fe and Mn was only observed in the shallowest trap at a depth of 214 m. Particulate Fe and Mn fluxes correlate at all sampled depths (Fig. 8C). The strength of the correlation

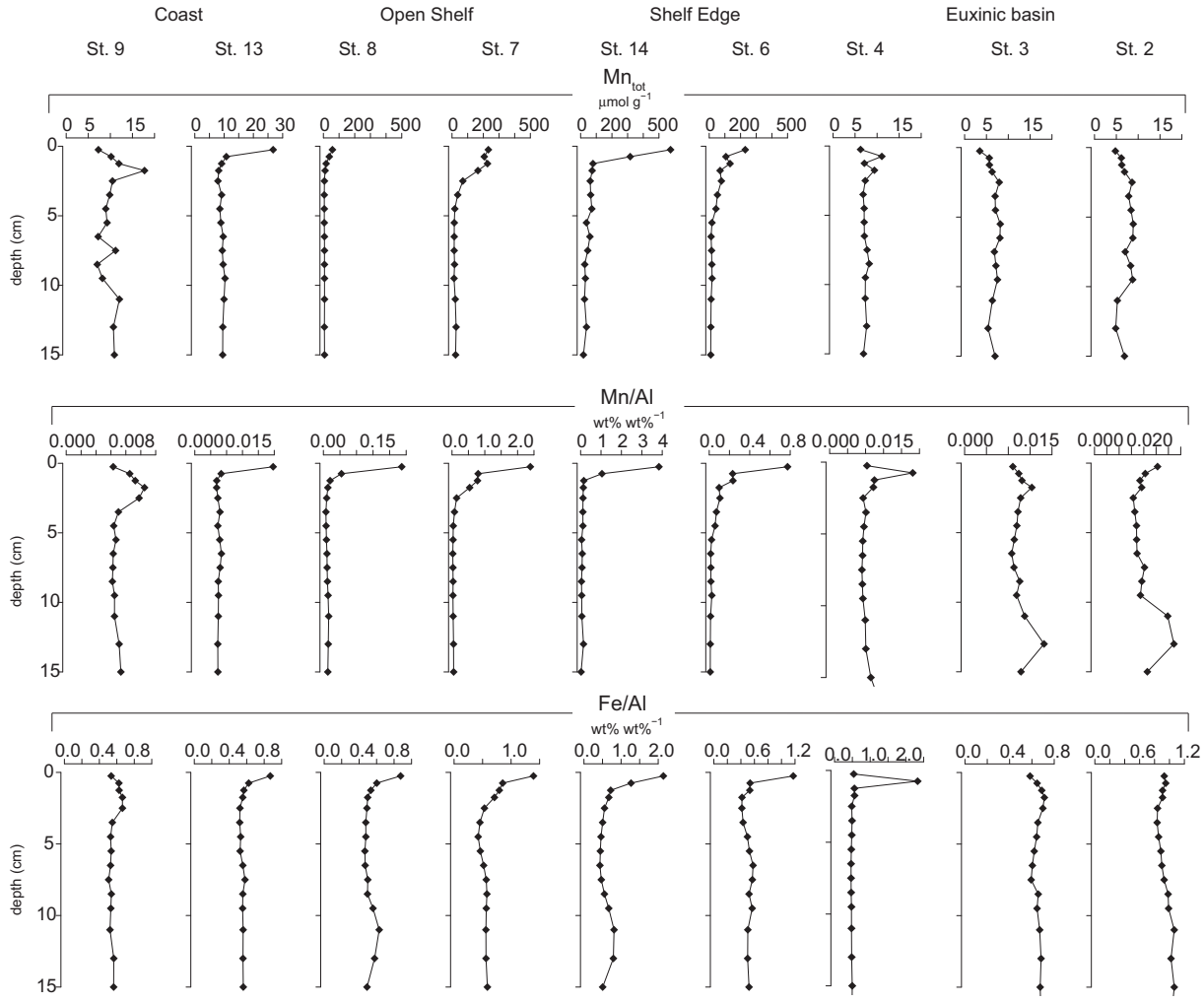

Fig. 4. Solid phase depth profiles of total Mn (Mn_{tot}), Mn/Al and Fe/Al at nine stations on the northwestern Black Sea shelf. Note the different x-axis scale.

increases with water depth (Fig. 8C). μXRF scanning of two subsamples from 214 m water depth revealed one area where Mn was enriched (Fig. A.6A). Within this area, Mn counts strongly correlated with Fe counts (Fig. A.6; R^2 = 0.985).

4. DISCUSSION

4.1. Sedimentary Mn release

Reduction of Mn oxides by microbial or chemical pathways is stimulated by the input of organic matter (Burdige, 1993). At our stations on the northwestern Black Sea shelf the input of organic matter decreases from the coast towards the shelf edge (Table 2; Wijsman et al. (1999); Lenstra et al., 2019). At the organic-rich coastal stations 9 and 13, high rates of sedimentary organic matter degradation are inferred from high rates of oxygen uptake and shallow oxygen penetration depths (>17 mmol m^{-2} d^{-1} and <3 mm, respectively; Table 2). At these stations, the shape of the porewater Mn profiles indicate Mn oxide reduction near the sediment surface (Fig. 2C). Bottom water oxygen concentrations at these stations were 92 and 209 µmol L^{-1}, respectively, and the surface sediments were oxygenated (Table 2). Nevertheless, high rates of benthic release of Mn were observed at these sites (up to 0.47 mmol m^{-2} d^{-1}; Fig. 2B; Table 3), indicating that oxidation of dissolved Mn in the surface sediment played only a minor role. This is likely related to the slow rates of oxidation of dissolved Mn (Nealson et al., 1988; Burdige, 1993; Luther, 2010).

Based on benthic flux measurements of Fe obtained in parallel to our *in-situ* flux measurements for Mn, it was previously proposed that macrofauna strongly enhanced the benthic release of Fe at stations 9 and 13 (Lenstra et al., 2019). This was deduced from a quantification of bioirrigation, using bromide as a tracer, highlighting relatively high rates of water exchange between sediment burrows and the overlying water at the time of sampling for this study (Lenstra et al., 2019). The *in-situ* benthic fluxes of Mn at our coastal stations are comparable in range to those determined previously in this region (0.31 and 0.42 mmol m^{-2}

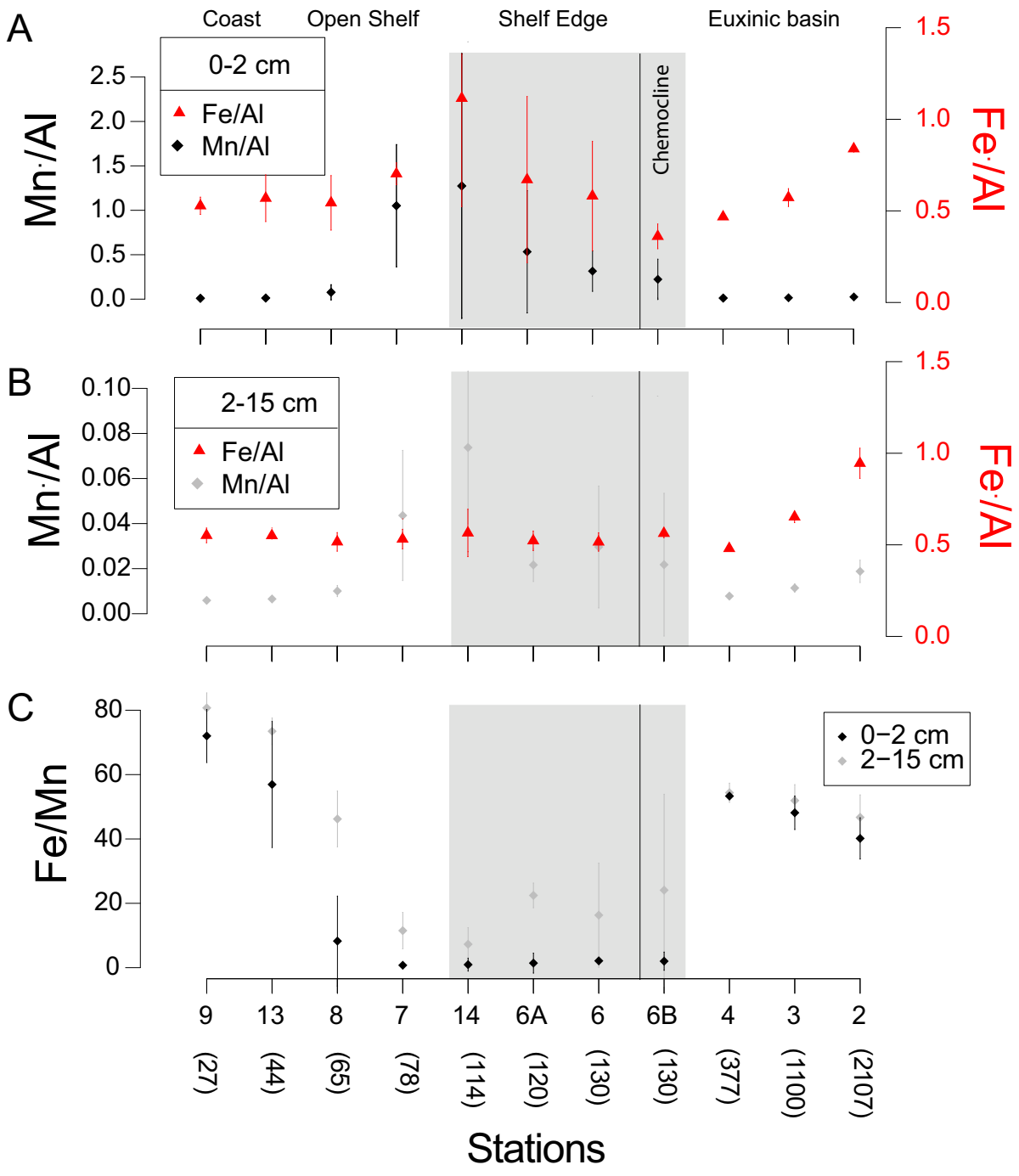

Fig. 5. Indicators for enrichment of Mn and Fe (Mn/Al and Fe/Al) in different depth intervals (Table 4). (A): Mn/Al and Fe/Al (0–2 cm); (B): Mn/Al and Fe/Al 2–15 cm. (C): Fe/Mn ratio.

d^{-1}; Friedrich et al. (2002)) and to those for bioirrigated sites with similar bottom water oxygen concentrations in Aarhus Bay (0.33–0.42 mmol m^{-2} d^{-1}; Thamdrup et al. (1994)). Enhanced benthic release rates of Fe and Mn along the Oregon and California continental shelf were also linked to macrofaunal activity (Berelson et al., 2003; Severmann et al., 2010; McManus et al., 2012). We conclude that, besides diffusion, bioirrigation plays a key role in the benthic release of Mn in the coastal zone of the northwestern Black Sea shelf.

At the open shelf and shelf edge where the organic matter flux is very low (Wijsman et al., 1999; Lenstra et al., 2019), there is little Mn mobilization in the sediment and only limited benthic release of Mn (<0.05 mmol m^{-2} d^{-1}; Table 3), despite the abundant presence of Mn oxides (Fig. 4). Thus, while dissolved Mn concentrations are

Table 4
Average values of sediment indicators for the enrichments of Mn and Fe (Mn/Al and Fe/Al) and Fe/Mn at eleven stations for depth intervals 0–2 and 2–15 cm in the sediment.

	Station	Mn/Al	Fe/Al	Fe/Mn
0–2 cm	9	0.0085	0.61	72
	13	0.011	0.65	56.9
	8	0.076	0.63	8.3
	7	1.05	0.79	0.7
	14	1.27	1.2	0.9
	6A	0.53	0.76	1.4
	6	0.31	0.67	2.1
	6B	0.01	0.45	2.0
	4	n.a.	0.55	53.3
	3	0.01	0.66	48.1
	2	0.023	0.92	40.2
2–15 cm	9	0.0068	0.55	80.7
	13	0.0075	0.55	73.5
	8	0.011	0.51	46.2
	7	0.046	0.53	11.5
	14	0.077	0.56	7.3
	6A	0.023	0.52	22.5
	6	0.031	0.51	16.3
	6B	0.023	0.56	24.1
	4	0.088	0.48	54.4
	3	0.013	0.65	51.9
	2	0.020	0.94	46.7

relatively high close to the sediment–water interface at the coastal, organic-rich stations 9 and 13, they are much lower in the organic-poor sediments elsewhere on the shelf (Fig. 2C). This emphasizes the importance of organic matter deposition for the mobilization of Mn in the sediment and subsequent benthic release of Mn, in accordance with earlier research (e.g. Slomp et al., 1997; McManus et al., 2012).

In the bottom waters of the euxinic deep basin, dissolved Mn concentrations in the porewater and in the water column are similar. Manganese oxides do not survive transfer through the euxinic water column (Yakushev et al., 2009; Dellwig et al., 2010; Dijkstra et al., 2018) and as a consequence, reductive dissolution of Mn oxides and production of dissolved Mn do not occur in the surface sediment.

4.2. Transport of Mn in the water column

Dissolved Mn in marine waters mainly consists of Mn (II) and Mn(III)-L (Faulkner et al., 1994; Sander and Koschinsky, 2011; Oldham et al., 2017). Particulate Mn is thought to predominantly consist of Mn oxides, Mn carbonates or Mn in clay and/or organic matter. The relative proportion of dissolved and particulate Mn may differ depending on the type of shelf environment (e.g. Vieira et al. (2019)). We find that in northwestern Black Sea shelf waters most Mn is present as dissolved Mn (<0.2 μm) near the seafloor, with concentrations of Mn in dissolved and particulate form (and TdMn) decreasing towards the shelf edge (Figs. 2A and 3A). These observations agree with trends in dissolved and particulate Mn reported for sites in a nearby area in the summer of 1995 (Tankéré et al., 2001), suggesting that this is a consistent feature of the northwestern Black Sea shelf. The high concentrations of dissolved Mn in the bottom waters in the coastal zone are likely the result of high benthic Mn release (Fig. 2).

Further off-shore, dissolved Mn remains the dominant Mn form in the oxygenated waters of the shelf (Fig. 2A; Table 3), despite the absence of a major benthic source of dissolved Mn. Since the kinetics of dissolved Mn(II) oxidation in seawater are quite slow (Stumm and Morgan, 1996; Luther, 2010; Von Langen et al., 1997; Tebo et al., 2005), some of this dissolved Mn could be Mn(II). Part of the dissolved Mn is likely also present as Mn(III) complexed by organic ligands, as shown recently for oxygenated coastal waters in the St. Lawrence Estuary (Oldham et al., 2017).

At the shelf edge station 6, Mn is predominantly present as particulate Mn, with dissolved Mn only accounting for 8% of the Mn in the water column (Fig. 2A; Table A.6). In this area, both diffusion and advection of dissolved Mn from the chemocline provide the main input of Mn to the water column (Figs. 2A and 3A; Brewer and Spencer (1974); Tebo, 1991). In contrast to the coastal zone, Mn does not remain in solution but mainly is present in the form of Mn oxides (Fig. 2A). We hypothesize that at the shelf edge, concentrations of organic ligands that are capable of stabilizing dissolved Mn are not high enough to prevent oxidative precipitation of dissolved Mn (Fig. 3C). An offshore decrease in the abundance of dissolved organic matter and humic substances is typical for river-dominated areas (Beck et al., 1974; Shiller et al., 2006; Oldham et al., 2017) and is thus in line with the suggested lateral trend in ligand-bound Mn.

Most of the particulate Mn in the water column on the shelf consists of easily reducible Mn oxides (Fig. 3). The deposition of Mn oxides from the water column is reflected in relatively high sedimentary Mn contents close to the sediment–water interface at the open shelf and shelf edge stations 7, 14 and 6 (Fig. 4). Results of XANES and

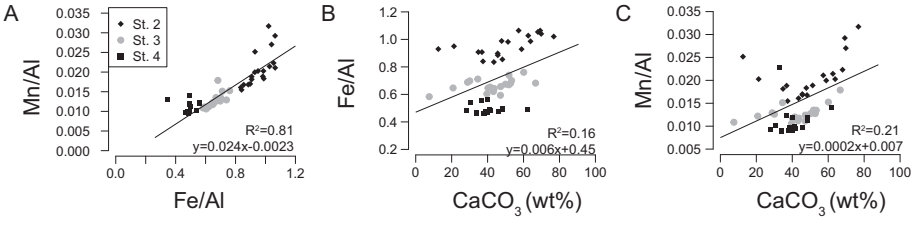

Fig. 6. (A): Fe/Al vs Mn/Al; (B): calcium carbonate ($CaCO_3$) versus Fe/Al and (C): $CaCO_3$ versus Mn/Al at three stations in the euxinic deep basin (0–26 cm depth). $CaCO_3$ in weight %.

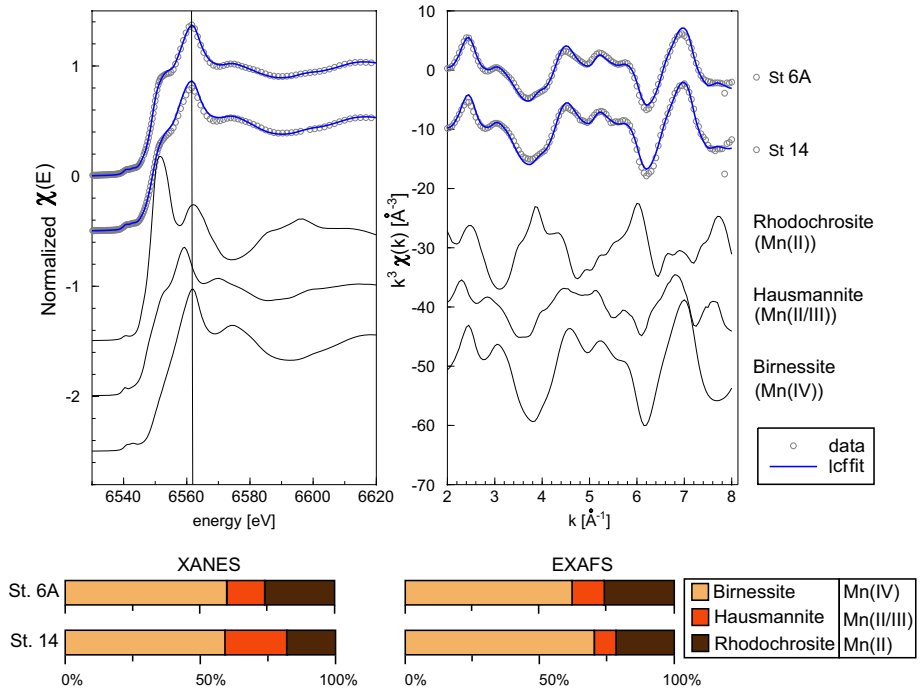

Fig. 7. Normalized XANES and k^3 weighted EXAFS spectra at the Mn K-edge obtained for sediment samples from the top 0.5 cm of stations 6A and 14. The circles show the data and the blue lines are the results from linear combination fitting (LCF). The black lines below represent the spectra of reference materials which were used for the LCF. The vertical line in the figure shows the position of the peak in the sample, which has a similar position as the peak in birnessite, and lies at a higher energy than the peak of hausmannite. Relative contributions of Mn (IV) (birnessite), Mn(II/III) (hausmannite) and Mn(II) (rhodochrosite) based on LCF are shown at the bottom of the figure. (For interpretation of the references to colour in this figure legend, the reader is referred to the web version of this article.)

EXAFS analyses for stations 14 and 6A indicate that the Mn oxides in the surface sediment predominantly consist of Mn(IV) oxides, possibly as birnessite (Fig. 7; Table 5). These oxides are mostly produced by microbial Mn(II) oxidation (Tebo et al., 2004; Santelli et al., 2011; Webb et al., 2005; Jürgensen et al., 2004). Birnessite can also be formed through photoinduced, abiotic Mn(II) oxidation (Jung et al., 2017; Learman et al., 2013) but this pathway is likely irrelevant for Mn oxidation in shelf sediments and the lower part of the water column in the Black Sea because of a lack of light. The Mn carbonate rhodochrosite is also present, but at lower concentrations. Upward diffusion of Mn from the porewater and subsequent oxidation can also contribute to the surface enrichments in Mn. The role of upward diffusion can be calculated from porewater profiles of Mn and rates of burial of Mn (Table A.7). At station 7, we find that upward diffusing Mn could account for up to 40% of the total surface enrichment. At the shelf edge stations 14 and 6, however, recycling of Mn in the sediment accounts for at most 13% of the enrichment, because of low porewater concentrations. We conclude that lateral inputs of Mn from the coastal zone and from the chemocline both contribute to high Mn contents at the shelf edge stations.

At the deep basin stations, concentrations of dissolved Mn were high in and below the chemocline, with relatively little particulate Mn being present (Fig. 2). The observed depth trends are in line with previous work on Mn in the Black Sea showing oxidation of dissolved Mn above the chemocline and reduction of Mn oxides in and below the chemocline (Spencer and Brewer, 1971; Tebo, 1991; Trouwborst et al., 2006; Dellwig et al., 2010; Dijkstra et al., 2018).

4.3. Mn dynamics in the deep basin and removal to the sediment

Dissolved Mn, present as Mn(II) (Trouwborst et al., 2006), accumulates in the waters of the euxinic basin below the chemocline (Fig. 2A). This is the result of rapid dissolution of Mn oxides in the sulfidic waters (Burdige and Nealson, 1986; Yakushev et al., 2009). Because typically only minor amounts of other particulate Mn forms are present, sediments underlying an euxinic water column are often depleted in Mn (Calvert and Pedersen, 1993; Brumsack, 2006; Lenz et al., 2015). However, we observe a strong correlation between particulate Mn and Fe in sinking material (Fig. 8), Mn and Fe in suspended matter from a sediment trap at the microscale (Fig. 6), and sediment Mn/Al and Fe/Al (Fig. 6) in the euxinic deep basin. This suggests coupled downward transport of Mn and Fe and possible coupled burial of Mn and Fe in the deep basin sediments.

A correlation between Mn/Al and Fe/Al in Black Sea sediments was observed earlier by Lyons and Severmann (2006). They hypothesized that, similar to Fe, Mn sulfides

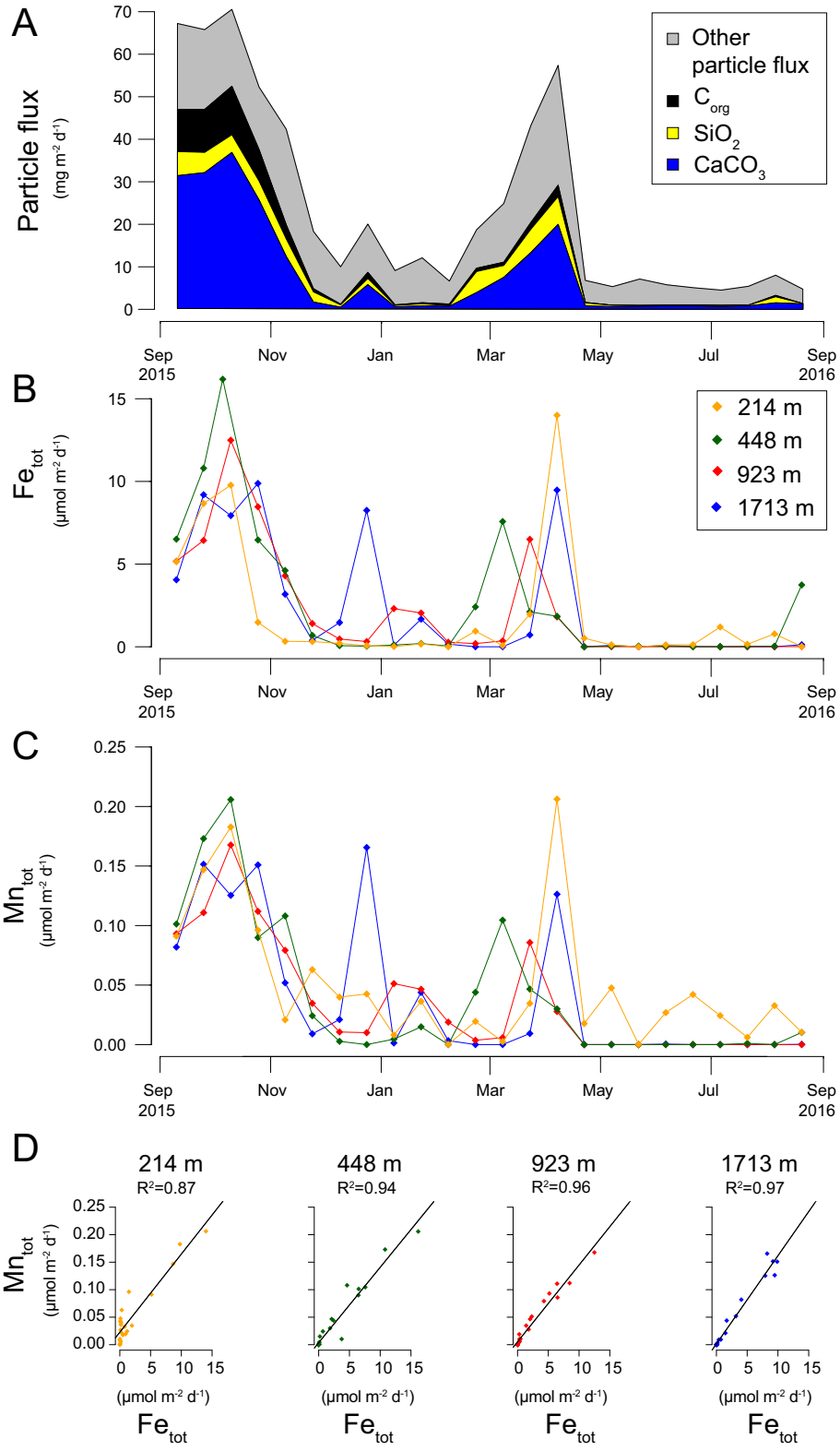

Fig. 8. Sediment trap derived downward fluxes at four water depths of (A): total particle flux, C_{org}, SiO_2 and $CaCO_3$; (B): iron (µmol m^{-2} d^{-1}); (C): Mn (µmol m^{-2} d^{-1}). (D): Correlation between particulate Fe and Mn in sediment traps at four different depths.

were formed in the water column and subsequently buried. Thermodynamic calculations indicate that Mn sulfide formation at water depths below 800 m in the Black Sea could be possible (Lewis and Landing, 1991; Landing and Lewis, 1991). While to date no evidence for Mn sulfides in the deep basin sediments has been found, results

Table 5
Relative contribution of Mn(IV) (birnessite), Mn(II/III) (hausmannite) and Mn(II) (rhodochrosite) (%) in the surface layer of the sediments at stations 14 and 6A (Fig. A.1) based on X-ray absorption spectroscopy.

	XANES				EXAFS			
	Mn(IV) birnessite (%)	Mn(II/III) hausmannite (%)	Mn(II) rhodochrosite (%)	R factor (10^3)	Mn(IV) birnessite (%)	Mn(II/III) hausmannite (%)	Mn(II) rhodochrosite (%)	R factor (10^3)
St. 14	59 ± 2	23 ± 2	18 ± 3	0.58	70 ± 20	8 ± 3	21 ± 3	37
St. 6A	60 ± 1	14 ± 10	26 ± 10	0.13	60 ± 1	15 ± 2	26 ± 2	20

The quality of the lcf fitting was evaluated based on the R-factor ($\sum$(data-fit)^2)/sum(data^2)). A R-factor below 0.05 is considered to reflect a reasonable fit (Kelly et al., 2008).

of X-ray spectroscopy recently revealed the presence of small amounts of Mn carbonate (Dijkstra et al., 2018). These Mn carbonates cannot be formed *in-situ*, however, because concentrations of dissolved Mn and the alkalinity in the euxinic water column and pore water are too low (Landing and Lewis, 1991; Calvert and Pedersen, 1993; Figs. 2A and A.7). Therefore, these Mn carbonates were likely formed on and transported from the continental shelf (Dijkstra et al., 2018). The lack of a consistent correlation between sediment Fe/Al and Mn/Al versus sediment $CaCO_3$ (Figs. 6B and C) suggests that the Fe and Mn enrichments are not directly related to variations in $CaCO_3$ input. Instead, we hypothesize that Mn becomes directly associated with Fe in pyrite in the water column. The association of Mn with sedimentary pyrite is known from the geological record (Large et al., 2014) and has been shown for modern sediments using sequential chemical extractions (Huerta-Diaz and Morse, 1990, 1992) scanning electron microscopy and energy dispersive spectroscopy (Lenz et al., 2014) and XANES analyses (Lenz et al., 2014; Hermans et al., 2019).

Continental shelves are the key source of reactive Fe in the euxinic deep basin of the Black Sea, with transport taking place through shelf to basin Fe shuttling and turbidite deposition (Wijsman et al., 2001; Raiswell and Canfield, 2012; Lenstra et al., 2019; Kraal et al., 2019). Periods of enhanced transport of reactive Fe from the continental shelf are recorded in the adjacent deep basin as Fe enrichments (Wijsman et al., 2001; Raiswell and Canfield, 2012; Eckert et al., 2013). In the euxinic basin, Fe oxides, which account for a major proportion of the reactive Fe, are rapidly converted to pyrite (Muramoto et al., 1991; Dijkstra et al., 2018). Most of the conversion of Fe oxides to pyrite occurs close to the oxic-anoxic interface in the water column (Muramoto et al., 1991; Lyons, 1997; Cutter and Kluckhohn, 1999), and as a consequence, concentrations of dissolved Fe decrease rapidly with water depth (Dijkstra et al., 2018). Downward transport of pyrite was previously suggested to occur through scavenging by organic matter in winter and spring after seasonal phytoplankton blooms (Muramoto et al., 1991). We find, however, that the flux of Fe correlates more strongly with the total particle flux than with the organic matter flux, although periods of high Fe flux only occur following phytoplankton blooms. This could imply that, for scavenging of pyrite, the nature of the settling material is less important than its quantity, if a minimum amount of organic matter is present (Fig. 8).

Water column Mn shows a similar trend with water depth as dissolved Fe and decreases from 8 to ca. 5 μmol L^{-1} below the chemocline (Fig. 2A). This suggests that dissolved Fe and Mn precipitate at approximately the same depth in the water column. Most of this decrease occurs above the part of the water column where supersaturation for Mn sulfide has been suggested (>800 m; Lewis and Landing (1991,)). We therefore propose that Mn may be incorporated in pyrite in the water column. Typically, such incorporation depends on the amount of pyrite produced or by the supply of dissolved Mn (Huerta-Diaz and Morse, 1990, 1992). Given the relatively low molar ratio of total Fe and Mn of 0.0054 in the water column (Table A.6), the incorporation of Mn is expected to be limited by the rate of pyrite formation. We conclude that the burial of Mn in the deep basin is likely controlled by the transport of reactive Fe from the continental shelf and subsequent pyrite formation in the water column. This explains the strong positive correlation between Fe and Mn in the deep basin sediments. Such a correlation may be typical for marine environments where sulfidic conditions in the water column are persistent and where syngenetic pyrite formation dominates.

4.4. Comparison of Fe and Mn shelf to basin shuttling

The rapid oxidation kinetics of dissolved Fe, compared to the slower, mainly bacterial mediated, oxidation of dissolved Mn (Stumm and Morgan, 1996; Tebo et al., 2005; Learman et al., 2011) contribute to differences in shelf to basin shuttling of Fe and Mn. This has implications for the transport of both metals in the water column and the sequestration and burial of Fe and Mn and associated elements (Koschinsky and Hein, 2003).

At the coastal stations in our study, the benthic release fluxes of Fe and Mn are approximately equal, despite 4.5-fold higher porewater concentrations of Fe, when compared to Mn (Fig. 9A). The oxic bottom waters prevent release of most of the porewater Fe by promoting its oxidation in the sediment, while dissolved Mn does make its way into the overlying water. In the water column, most Fe is in the form of Fe oxides (Lenstra et al., 2019), while the Mn remains in dissolved form, likely bound to ligands (Oldham et al. (2019); Fig. 9). As a consequence, the sus-

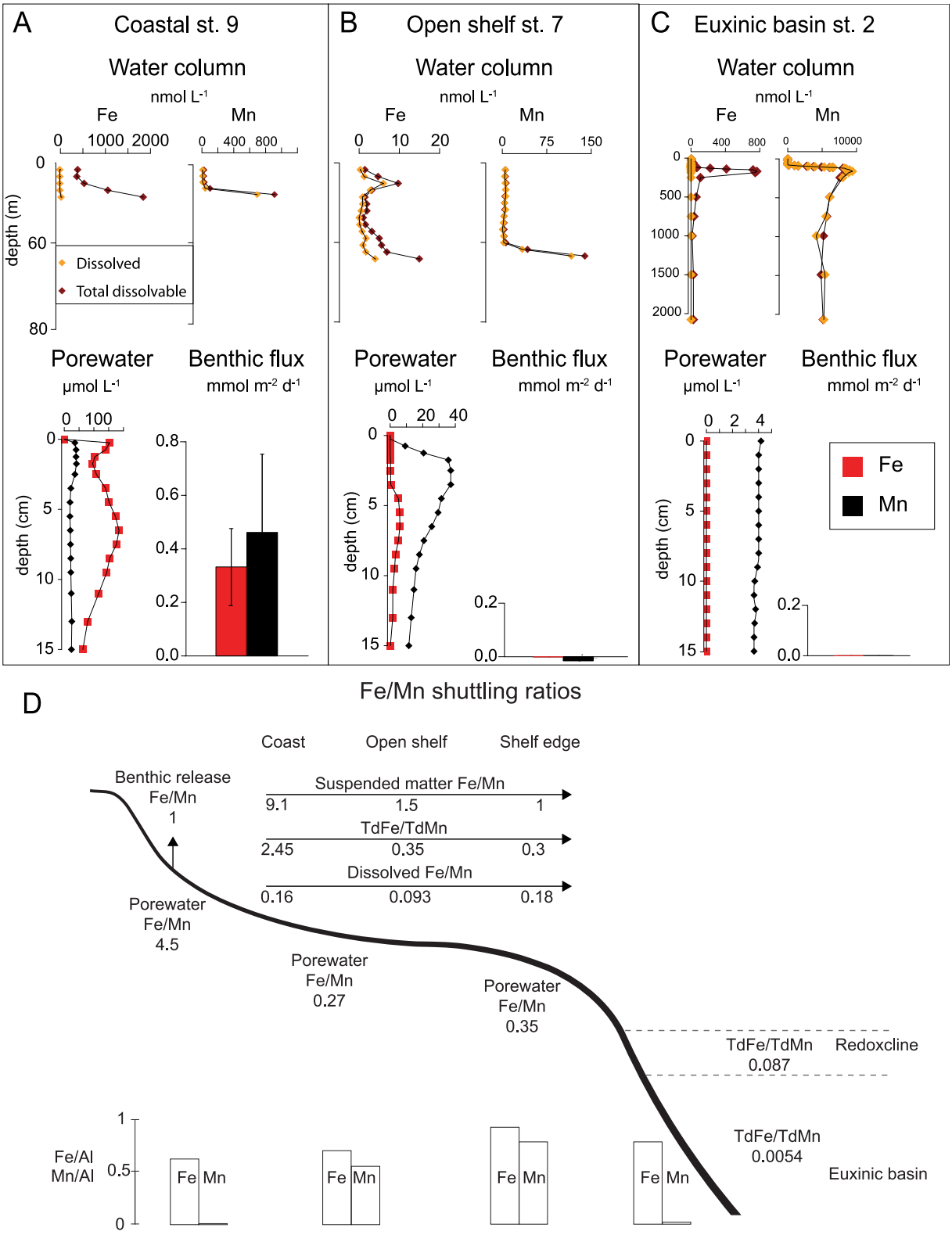

Fig. 9. Comparison of water column and pore water Fe and Mn and benthic release of Fe and Mn: (A): coastal zone (st. 9); (B): open shelf (st. 7) and (C): euxinic basin (st. 2). Benthic release in the deep basin is based on calculated diffusive fluxes (Table 3). Iron data are from (Lenstra et al., 2019). (D): ratio of Fe/Mn (mol/mol) over the northwestern Black Sea shelf. All ratios are calculated as average for over two stations (coastal stations: 9 and 13, open shelf stations: 8 and 7 and shelf edge stations: 14 and 6). Porewater Fe/Mn based on the maximum concentrations in the first 15 cm. Water column Fe/Mn is based on the deepest filter and deepest sample in the water column. Sediment Fe/Al and Mn/Al for the first two centimeter in the sediment are shown. Data for individual stations are in Tables 4 and A.6.

pended matter in the water column is enriched in Fe relative to Mn (Fe/Mn ratio of 9.1), whereas little dissolved Fe is present relative to Mn (Fe/Mn ratio of 0.16). The difference in mobility of Fe and Mn explains why the coastal sediments contain relatively little Mn to Fe (Figs. 5 and 9D): while Fe is trapped by oxidation and the Fe oxides formed are converted to Fe sulfides at depth (Lenstra et al., 2019), most incoming Mn is lost to the water column.

At the open shelf and shelf edge stations, little benthic release of either Fe or Mn is observed (Fig. 9B and D). Here, porewater concentrations of both Fe and Mn are low, but Mn dominates over Fe. Both elements are recycled

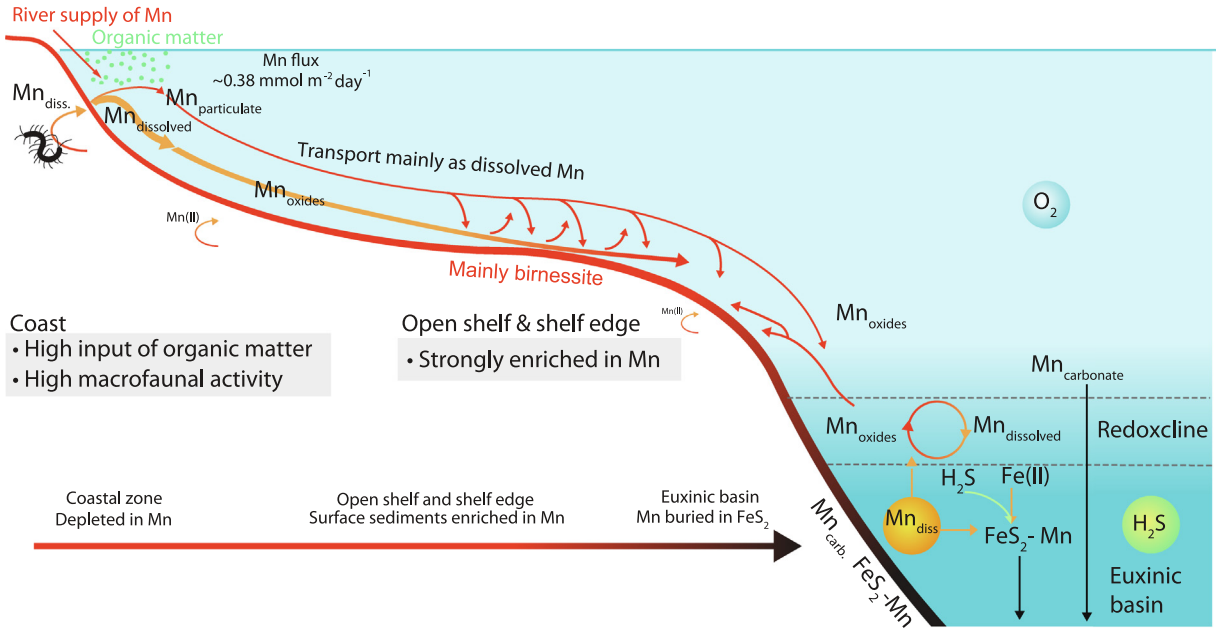

Fig. 10. Schematic overview of Mn shuttling on the northwestern Black Sea shelf. Red lines and arrows indicate particulate Mn (>0.2 μm), orange arrows indicate dissolved Mn (<0.2 μm). (For interpretation of the references to colour in this figure legend, the reader is referred to the web version of this article.)

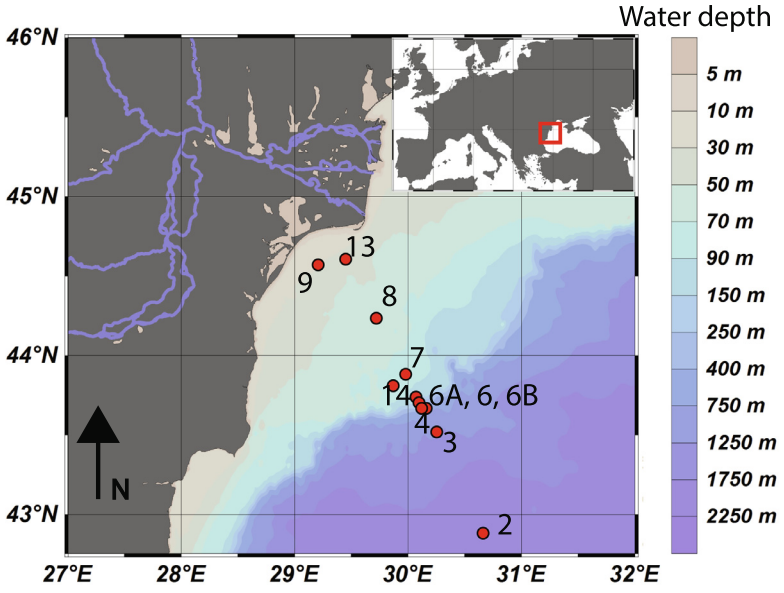

Fig. A.1. Locations of the eleven stations sampled on the northwestern Black Sea shelf and in the deep basin when including the stations from Kraal et al. (2017) (Table A.1).

in the porewater below the surface sediment. In the water column, Mn also gains quantitative importance over Fe, not only in suspended matter (Fe/Mn ratio of 1.5 to 1), but also in dissolved form (Fe/Mn ratio of 0.093 to 0.18; Fig. 9). In the surface sediment, total Fe and Mn concentrations are relatively close (Fe/Mn = 0.8). As discussed by Lenstra et al. (2019), the major source of Fe on this outer part of the shelf is riverine, with subsequent mobilization of Fe in bioirrigated coastal sediments and cross-shelf transport of Fe in suspended matter. While the same mechanisms of mobilization are at work for Mn in the coastal zone, its higher mobility in the water column leads to transport over greater distances over the shelf when compared to Fe. On the Black Sea shelf, this higher mobility is likely the combined result of slower oxidation of dissolved Mn, more limited sequestration of dissolved Mn in the sediment and more effective complexation of Mn as Mn(III) with organic ligands, when compared to dissolved Fe. Notably, Mn and Fe bind to the same ligands, but Mn complexes are often thermodynamically more stable and Mn(III) complexation is thought to be favored over complexation of dissolved Fe (Oldham et al., 2017). This allows the Mn to remain in dissolved form, typically in the <0.02 μm fraction, allowing the Mn to be transported further than the Fe, which is largely in particulate form (>0.2 μm). Importantly, the chemocline likely contributes more Mn to shelf edge sediments than Fe, given the much higher dissolved Mn concentrations than Fe in the waters that impinge upon the shelf (Fe/Mn ratio of 0.087; Fig. 9D).

Below the chemocline, the proportion of Fe relative to Mn in the euxinic water column decreases further because of effective sequestration of Fe in sulfides (dissolved Fe/Mn ratio of 0.0054; Fig. 9D). If, as we suggest, Mn is incorporated in pyrite in the water column, more dissolved Mn should ultimately be scavenged by pyrite with increasing water depth, leading to lower Fe/Mn ratios. Indeed, we see such a decline in sediment Fe/Mn from station 4 (377 m) to station 2 (2107 m; Fig. 5), in line with the proposed mechanism.

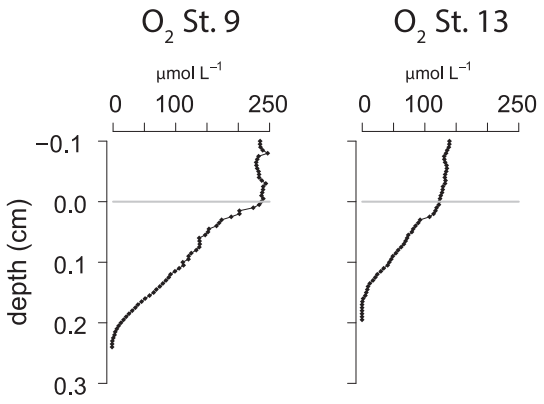

Fig. A.2. Porewater depth profiles of oxygen at stations 9 and 13 determined using micro-electrodes. Gray line indicates the sediment water interface. Data are from Lenstra et al. (2019).

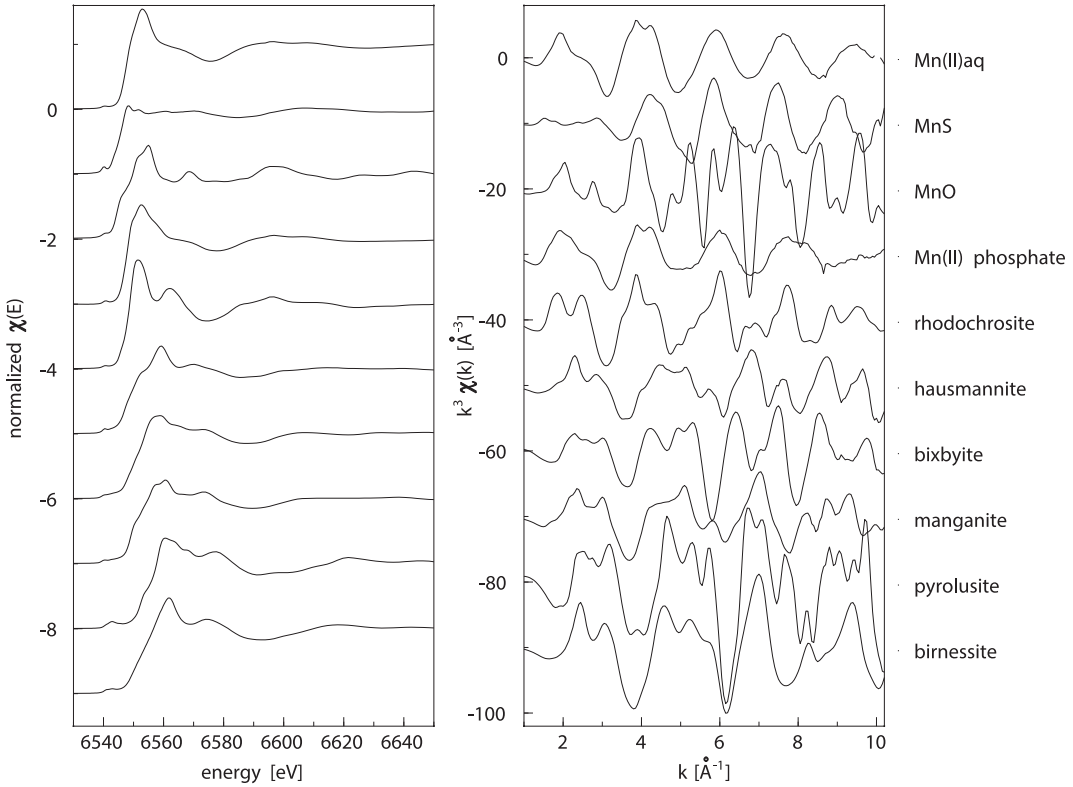

Fig. A.3. XANES (left panel) and EXAFS (right panel) spectra of reference materials used for the combinatorics fitting. The origin of the materials is presented in Table A.3.

In summary, we find that the differences in mobility of Fe and Mn promote lateral transport of Mn over Fe in Black Sea continental shelf waters. This leads to an enrichment in Mn relative to Fe in the waters and suspended matter of the open shelf and shelf edge. The stability of large amounts of reactive Mn oxides in the surface sediments on the open shelf and shelf edge is likely the direct result of the low organic matter input in this region, as observed previously for Fe (Lenstra et al., 2019). The contrasting modes of transport of Fe and Mn in the water column, i.e. through physical transport in particulate and dissolved form, respectively, has consequences for the transport of other elements across the shelf. While transport of elements that are primarily associated with Fe oxides will be promoted (e.g. phosphorus (P), arsenic and chromium; Koschinsky and Hein (2003)), the cross-shelf transport of elements that are mainly associated with Mn oxides (e.g. Co, zinc and Nickel (Ni); Koschinsky and Hein (2003)) could be decoupled from that of Mn.

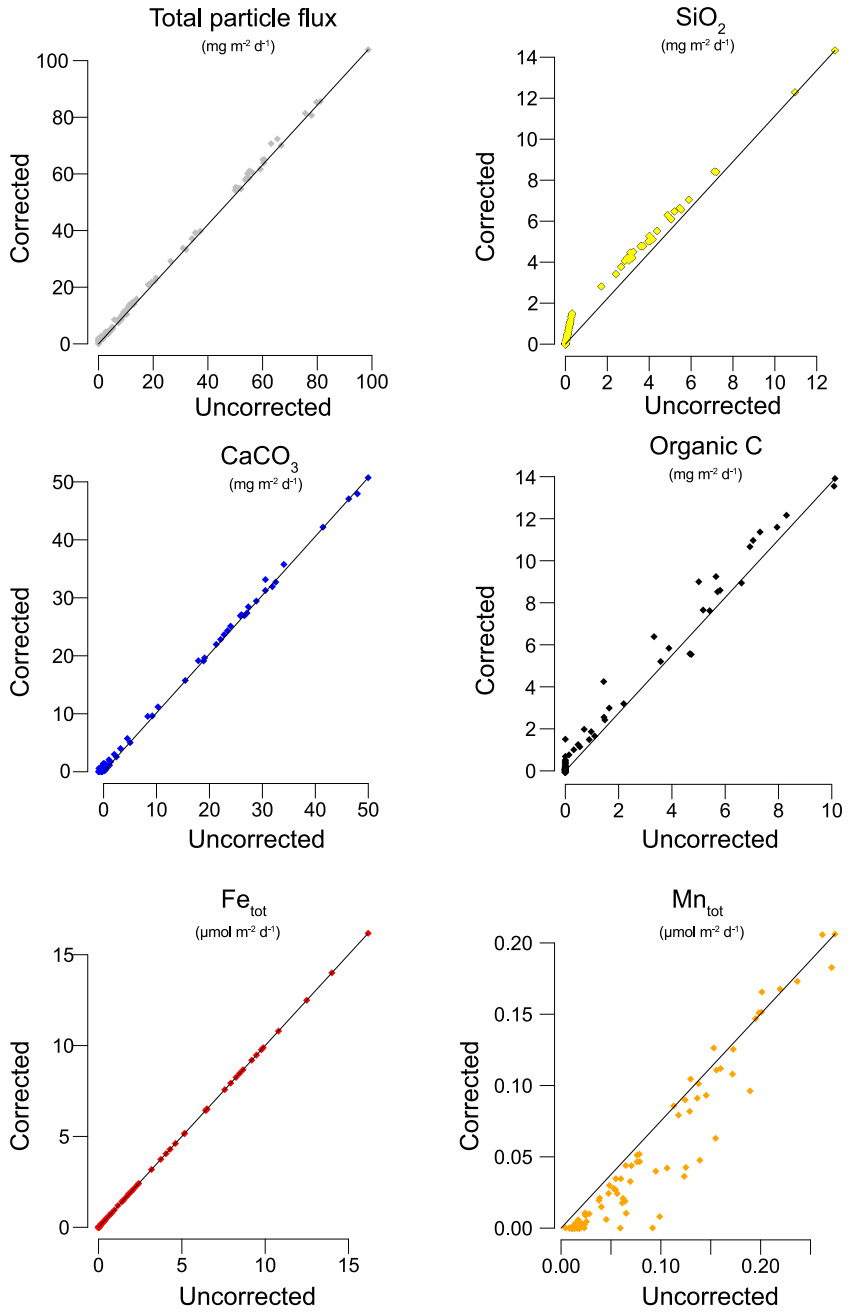

Fig. A.4. Comparison between uncorrected downward fluxes and corrected downward fluxes for total particle flux, SiO_2, $CaCO_3$, organic C, Fe_{tot} and Mn_{tot}.

4.5. Implications and conclusions

Sediments on continental shelves can act as an important source of Mn to the water column (Homoky et al., 2016). Release of Mn from sediments is thought to be highly dependent on the carbon oxidation rate in the sediment (McManus et al., 2012) and on bottom water redox conditions (Stumm and Morgan, 1996; Luther, 2010). We observe high Mn mobilization in the sediment and high benthic release of Mn from coastal sediments overlain by oxic bottom waters (up to 0.47 mmol m^{-2} d^{-1}; Table 3) in the Black Sea. We attribute this release to both diffusive and bioirrigative release of dissolved Mn, which is in accordance with high carbon oxidation rates and the high macrofaunal density and activity observed at these sites (Lenstra et al., 2019). This implies that sediments overlain by an oxic water column can act as an important source of Mn for the water column, thereby driving the Mn shelf to basin shuttle. This is line with previous work for shelf sediments as observed for the Oregon-California continental shelf by McManus et al. (2012). However, benthic fluxes of Mn in the Black Sea are notably higher (ca. 7 times). A schematic overview of Mn shuttling in the northwestern Black Sea shelf and euxinic deep basin is presented in Fig. 10.

Release of Mn from continental shelves at the global ocean scale was recently estimated at 3.4 ± 0.1 *Gmol* yr^{-1}, which is lower than the Mn input from dust of 5.6 ± 0.28 *Gmol* yr^{-1} (van Hulten et al., 2017). In this model calculation, van Hulten et al. (2017) assumed a similar Fe/Mn ratio for shelf porewaters and the corresponding benthic flux. This Fe/Mn ratio was set to a value of 5 based on Fe and Mn porewater data of North Sea shelf sediments (Slomp et al., 1997). The benthic Mn flux in the model was then directly calculated from that of Fe, leading to a 5-fold lower global Mn flux compared to that of Fe (van Hulten et al., 2017). The results for our coastal sites show that, despite nearly 5-fold higher porewater concentrations of Fe relative to Mn, equal amounts of both metals were released from the sediments to the overlying water (Fig. 10). This implies that the Fe/Mn ratio of 5 used by van Hulten et al. (2017) may be too high. As a consequence, the role of sediments as a source of Mn at the global scale may be underestimated.

We find that most of the Mn in Black Sea shelf waters is present in dissolved form, while most Fe is present as particulate Fe oxides (Lenstra et al., 2019). This implies that Mn is more easily transported through the water column compared to Fe. Additionally, Mn oxides are known to scavenge trace metals (e.g. Co, Ni and molybdenum, Shaw et al. (1990), Algeo and Tribovillard (2009)) and phosphate (Dellwig et al., 2010) from marine waters. A particulate Mn shuttle can therefore transport trace metals and P over the continental shelf and into deep basins (Dellwig et al., 2010; Scholz et al., 2013; Jilbert and Slomp, 2013; Little et al., 2015). The low concentrations of particulate Mn in Black Sea shelf waters suggest that scavenging and lateral transfer of trace metals and P by Mn oxides in the water column on the shelf is largely decoupled. This is different at the shelf edge, where Mn oxides dominate over dissolved Mn, and scavenging of trace metals and P from the water column and subsequent enhanced downward transport of metals and P into the euxinic basin becomes a possibility.

Where the chemocline in a euxinic basin impinges on shallower sediments, the Mn oxide content can be enhanced in a so-called "Mn bathtub ring" (Force and Cannon, 1988). In such sediments, Mn is typically buried as Mn carbonates upon Mn oxide dissolution at depth in the sediment (Brown et al., 2000; De Lange et al., 2008). We find that, at the shelf edge, surface sediments were indeed strongly enriched in total Mn, which was mostly in the form of Mn(IV) oxides (Figs. 4 and 7). Little of this Mn is buried, however, as is evident from the steep decline in total Mn with depth and the low concentrations of Mn at depth (<20 μmol g^{-1}; Fig. 4). At these stations the input of organic matter is low (Lenstra et al., 2019), resulting in limited conversion of Mn oxides to Mn carbonates and subsequent burial of Mn. This highlights that a Mn bathtub ring will only form in the presence of suitable organic matter deposition, corresponding alkalinity generation and eventu-

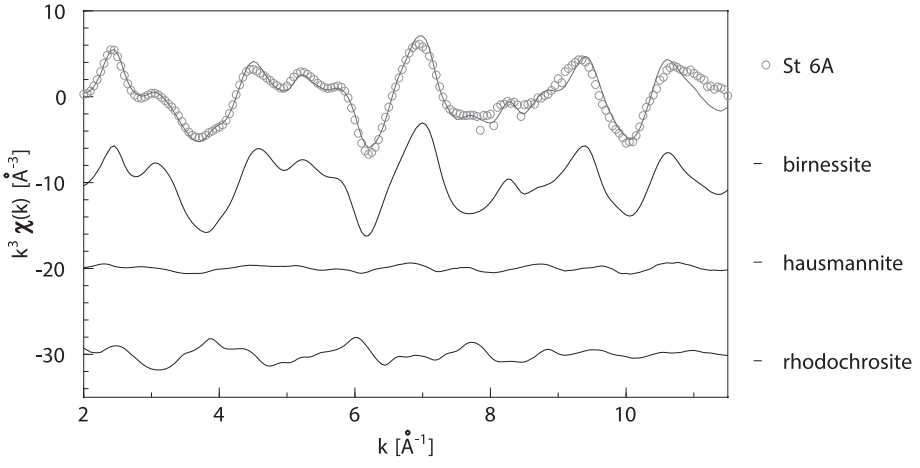

Fig. A.5. Results of linear combination fitting of the EXAFS spectrum of sediments from station 6A in the k-range 2–11 Å. The blue line represents the fitting result and the black lines the contribution from the three reference spectra.

ally Mn carbonate formation. Therefore, in the geological record, the presence of such a redox boundary may not always be recorded in the sediment by a Mn enrichment.

Sediments overlain by permanently anoxic/euxinic bottom waters typically contain little authigenic Mn (Calvert and Pedersen, 1993; Brumsack, 2006). We find that, in the

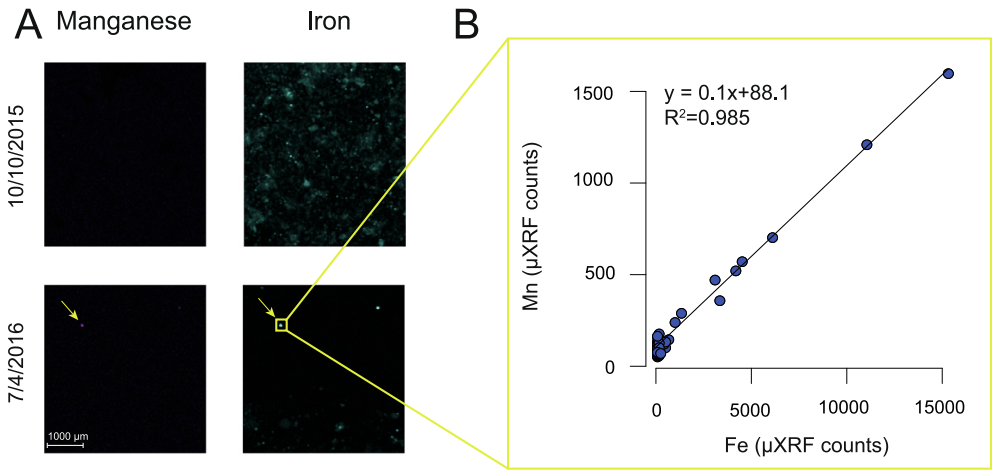

Fig. A.6. A: μXRF based elemental maps of Mn and Fe in suspended material collected with a sediment trap located at 215 meter water depth at two time points. B: correlation between Mn and Fe of μXRF counts within the yellow square. (For interpretation of the references to colour in this figure legend, the reader is referred to the web version of this article.)

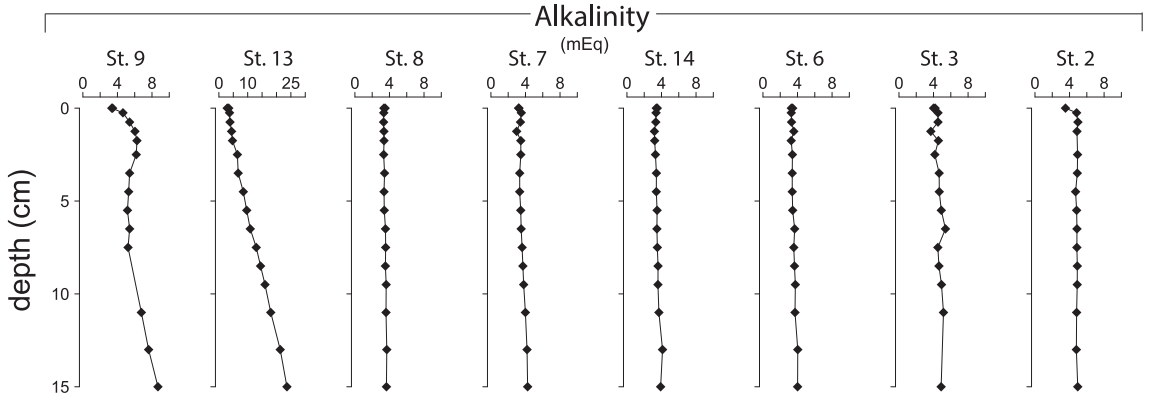

Fig. A.7. Porewater depth profiles of alkalinity at stations 9, 13, 8, 7, 14, 6, 3 and 2. Porewater alkalinity depth profiles for station 3 and 2 are from (Kraal et al., 2017).

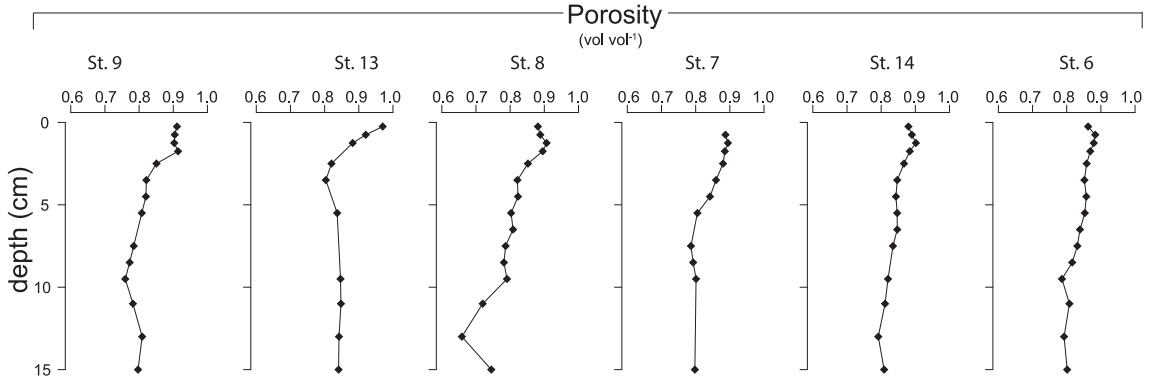

Fig. A.8. Depth profiles of porosity at stations 9, 13, 8, 7, 14 and 6.

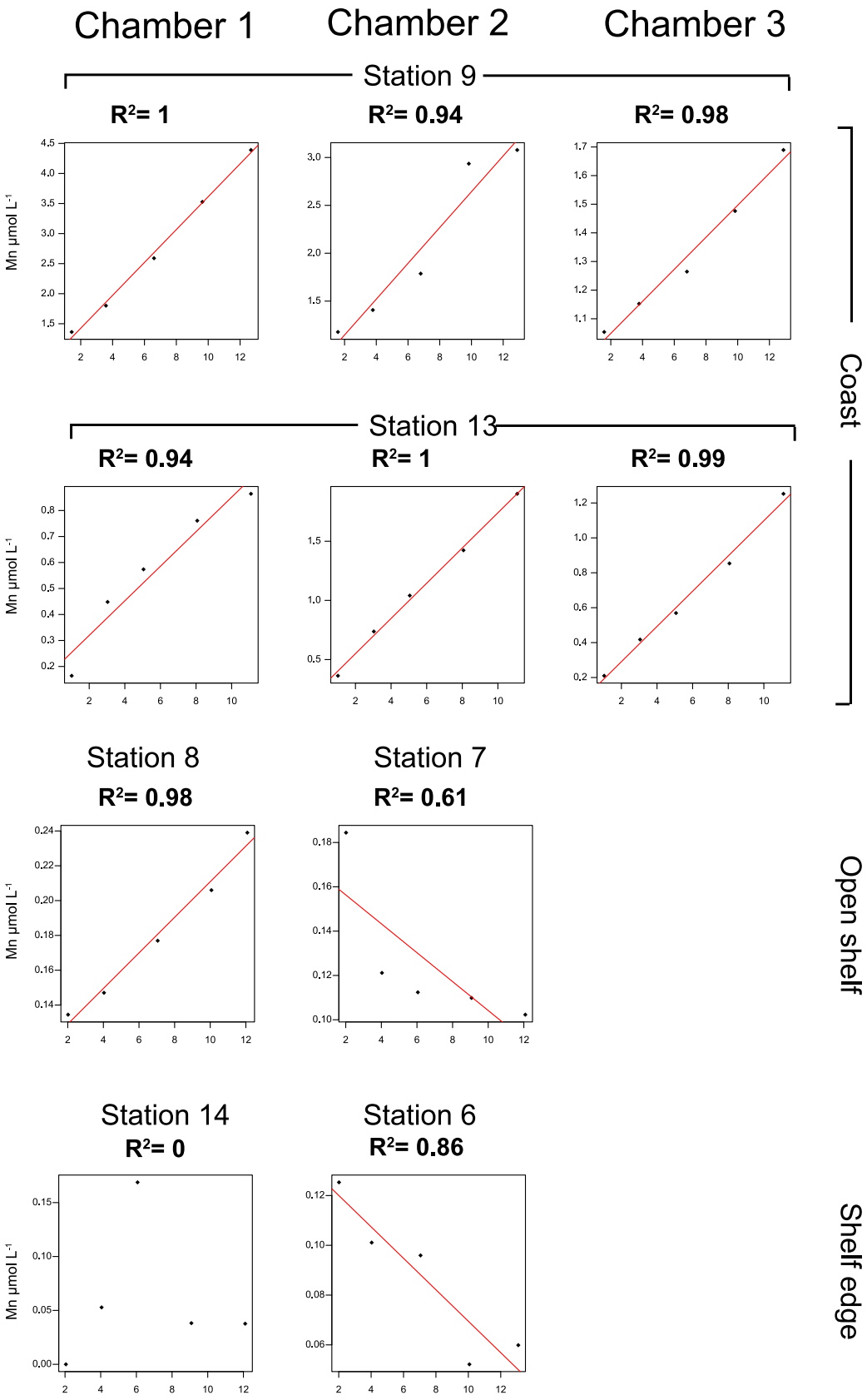

Fig. A.9. Total Mn concentration in benthic lander chambers versus time. Fluxes were calculated using linear regression (red line). Only regressions with $R^2 > 0.3$ were considered following Friedrich et al. (2002).

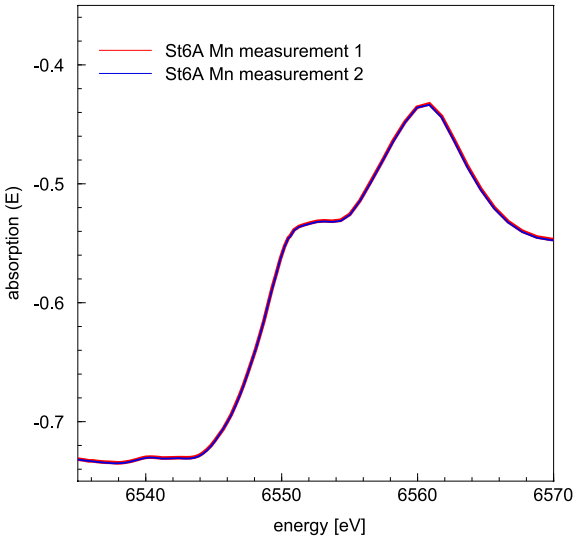

Fig. A.10. Two consecutively taken XANES spectra of the sediment sample from station 6A. The measurements were highly reproducible and no indications for photo-induced artifacts were observed.

euxinic basin of the Black Sea, sediment Mn is slightly enriched over a detrital background (Fig. 5B). In both sediment trap material and in the sediment, Mn/Al strongly correlates with Fe/Al (Fig. 6A; Table 4). This could be due to incorporation of Mn in pyrite in the water column. While further work is needed, this suggests that sediments where both Fe/Al and Mn/Al are enriched might be used to identify periods of euxinic waters from the geological record.

Declaration of Competing Interest

The authors declare that they have no known competing financial interests or personal relationships that could have appeared to influence the work reported in this paper.

ACKNOWLEDGEMENTS

We thank the captain, crew, technicians, Silke Severmann, Amy Kuzminov, Peter Kraal and all other scientists on board *R/V* Pelagia during cruises 64PE401 and 64PE418 for their assistance and Helen de Waard, Thom Claessen and Coen Mulder for analytical assistance in Utrecht. We thank Nina Papadomanolaki and her aid in retrieving the sediment trap samples. We thank three review-

Table A.1
Coordinates, water depth, bottom water temperature and H_2S at the 3 stations sampled on the northwestern Black Sea shelf and in the deep basin in June 2013 (Kraal et al., 2017). Unit mbss is meters below sea surface. n.a.: not available.

Station	Latitude N	Longitude E	Depth mbss	Temperature °C	BW H_2S µmol L^{-1}	Year
6A	43°44.1′	30°04.4′	120	8.5	0	2013
6B	43°42.8′	30°05.1′	130	8.5	0	2013
4	43°40.6′	30°07.5′	377	8.8	8.1	2013

Table A.2
Sequential extraction procedure for Mn as performed on suspended matter (steps 1 to 4) and sediment samples (steps 2 to 4) based on the Fe extraction procedures of Poulton and Canfield (2005), Claff et al. (2010) and Raiswell et al. (2010). Manganese associated with clays could also be extracted in step 3 and 4, therefore concentrations of reducible (crystalline) Mn oxides could be slightly overestimated.

Step	Extractant	Time (hours)	Target Fe phase	Target Mn phase	Label
1	0.17 M sodium citrate, 0.6 M sodium bicarbonate and 0.057 M ascorbic acid (pH 7.5)	24	Ferrihydrite	Easily reducible Mn oxides	$Mn_{Asc.}$
2	1 M HCl	4	Easily reducible Fe oxides Fe carbonates and FeS	Easily reducible Mn oxides Mn carbonates	$Mn_{Ox+Carb}$
3	50 g L^{-1} sodium dithionite solution buffered to pH 4.8 with 0.35 M acetic acid/ 0.2 M sodium citrate	4	Reducible (crystalline) Fe oxides	Reducible (crystalline) Mn oxides	Mn_{Ox2}
4	0.2 M ammonium oxalate 0.17 M oxalic acid (pH 3.2)	6	Magnetite	Reducible (crystalline) Mn oxides	Mn_{Ox2}

Table A.3
List of reference materials used for the linear combination fitting.

Mn phase	Source	Evaluation
MnO_2, pyrolusite	Alfa Aesar	XRD
MnO_2, hexagonal birnessite	In house: Mn oxide formed by oxidation of Fe(II) by Pseudomonas putida	EXAFS fitting
Mn^2O_3, bixbyite	Alfa Aesar	XRD
MnOOH, manganite	Waard	XRD
Mn_3O_4, hausmannite	In house: Abiotic oxidation of dissolved Mn(II)	XRD
MnO, manganosite	Alfa Aesar	XRD
$MnCO_3$, rhodochrosite	Baker	XRD
Mn(II)(aq)	In house: $MnSO_4$ solution	
Mn(II) phosphate, predominately hureaulite	Alfa Aesar	XRD
MnS, rambergite	In house: Mn(II) precipitated with S(-II)	EXAFS fitting

Table A.4
Speciation of Mn in suspended matter collected through *in-situ* filtration at stations 9, 13, 8, 7, 14 and 6. Mn extracted as in ascorbate acid (Asc. Mn), HCl (HCl Mn), citrate-dithionite bicarbonate (CDB Mn) and oxalic acid (Oxal. Mn) (Table A.2).

Station	Depth m	Volume filtered L	Asc. Mn nmol L^{-1}	HCl Mn nmol L^{-1}	CDB Mn nmol L^{-1}	Oxal. Mn nmol L^{-1}
9	10	36	6.7	0.9	2.4	8.1
	25	25	64.1	69.7	19.5	52.1
13	10	78	5.0	0.5	1.2	3.8
	39	91	30.8	5.9	2.4	5.3
8	10	126	3.1	0.3	0.7	2.4
	25	42	2.3	0.3	1.8	6.9
	35	8	11.0	1.5	11.	35.4
	55	183	23.5	3.5	1.0	2.3
7	10	220	1.1	0.1	0.4	1.3
	25	579	0.1	0	0.1	0.5
	35	328	0	0	0.3	0.9
	70	243	7.2	0.9	0.5	1.3
14	20	300	0.2	0	0.3	1.0
	40	579	0.7	0.1	0.2	0.6
	70	328	4.5	0.4	0.3	0.9
	90	243	7.9	1.1	0.5	1.3
6	20	120	0.3	0	0.7	2.4
	40	273	0.8	0.1	0.3	1.0
	80	379	2.6	0.3	0.2	0.8
	120	216	44.1	4.7	0.9	1.8

Table A.5
Relative contribution of Mn(IV) (birnessite), Mn(II/III) (hausmannite) and Mn(II) (rhodochrosite) (%) in the surface layer of the sediments at stations 6A (Fig. A.1) based on EXAFS fitting for two different k-ranges.

	range $Å^{-1}$	EXAFS Mn(IV) birnessite (%)	Mn(II/III) hausmannite (%)	Mn(II) rhodochrosite (%)	R factor (10^3)
St. 6A	2–8	60 ± 1	15 ± 2	26 ± 2	20
St. 6A	2–11	62 ± 1	11 ± 2	27 ± 2	44

Table A.6
Comparison of Fe and Mn dynamics along a water depth transect in the Black Sea. Max PW is the maximum concentration of Fe and Mn measured in the porewater (0–15 cm). Benthic release of Fe and Mn. Total water column is the concentration of total Fe and Mn in the deepest water column sample. Dissolved fraction is the fraction of dissolved Fe and Mn in the deepest water column sample. Solid phase Fe and Mn was averaged over the first two centimeter in the sediment. Suspended matter (SPM) Fe and Mn refers to the Fe and Mn in suspended matter in the deepest filter in the water column. Water column Fe/Mn refers to the ratio of total Fe and Mn in the deepest water column sample.

	Max PW		Benthic release		Water column		Dissolved	Fraction	Solid phase	Enrichment	SPM		Water column
Station	Fe(II) $\mu mol\ L^{-1}$	Mn(II) $\mu mol\ L^{-1}$	Fe $mmol\ m^{-2}\ d^{-1}$	Mn $mmol\ m^{-2}\ d^{-1}$	TdFe $nmol\ L^{-1}$	TdMn $nmol\ L^{-1}$	Fe %	Mn %	Fe $\mu mol\ g^{-1}$	Mn $\mu mol\ g^{-1}$	Fe $nmol\ L^{-1}$	Mn $nmol\ L^{-1}$	TdFe/TdMn fraction
9	185	41	0.34	0.47	1868	911	2	76	823	12	3217.4	205.4	2.1
13	213	74	0.38	0.3	495	174	5	55	792	14	111.8	44.5	2.8
8	25	65	0.037	0.03	46	81	25	96	372	31	42.3	45	0.6
7	6	37	0	−0.02	16	140	28	84	201	207	11	5.5	0.1
14	14	26	0.068	0	11	29	14	18	359	261	10.4	8.5	0.4
6	3	19	−0.19	−0.02	19	79	2	8	297	134	22.9	27.7	0.2
3	0	4	n.a.	n.a.	17.7	4242	100	100	267	4	n.a.	n.a.	0.0042
5.3	0	4	n.a.	n.a.	27.7	5139	100	100	272	6	n.a.	n.a.	0.0054

ers for insightful comments that greatly improved the manuscript. This research was funded by the Netherlands Organisation for Scientific Research (NWO-Vici grant 865.13.005, to CPS). We further thank the staff of the DUBBLE beamline (BM26a) at the European Synchrotron Radiation Facility (ESRF) and local contact Dipanjan Banerjee. Funding at the DUBBLE beamline was granted by the Netherlands Organisation for Scientific Research (NWO experiment 26–554 01–1094).

APPENDIX A

A.1. Benthic lander

During the benthic lander incubation, water samples were taken simultaneously with 30 mL plastic syringes connected to inlet ports inside and outside the incubation chamber after 2, 4, 7, 10 and 13 h. Each time a water sample was taken from the chamber, an equivalent volume of surrounding bottom water was allowed to enter the chamber. Upon lander retrieval from the seafloor the water samples were directly transferred to a temperature controlled laboratory maintained at *in-situ* temperature, acidified with 10 μL 10 M suprapur HCl per mL of sample and stored at 4 °C. TdMn in the samples was determined through ICP-MS using the SC-DX SeaFAST S2, as for water colum samples. Fluxes of Mn across the sediment–water interface were determined by fitting a linear regression to the concentration time series from each chamber (after correction for the dilution with the bottom water during each sampling interval). Only regressions with $R^2 > 0.3$ were considered, following Friedrich et al. (2002) (Fig. A.9). Calculated Mn fluxes for the different incubation chambers were averaged for each station. At stations 8, 7, 14 and 6, the benthic release of TdMn was determined with one chamber.

A.2. Energy calibration and data collection

Energy calibration was performed by assigning an energy of 7112 eV to the first maximum of the derivated spectrum of Fe(0) foil. Fe(0) foil was used for energy calibration as the collection of Mn spectra was combined with X-ray spectroscopy at the Fe K edge during the same experiment. Data were collected with a step size of 3 eV, 0.3 eV, and, with increasing energy, 1–3 eV, for the pre-edge, edge, and post-edge region of the spectra, respectively. Two spectra were collected for each sample and combined in χ(E). Two consecutive scans of sample from station 6A show no indications for photoreduction (Fig. A.10).

A.3. Linear combination Fitting

The set of spectra from reference material, used for the LCF of the Mn XAS spectra, is presented in Fig. A.3 and Table A.3. Using the combinatorics option in Athena, the best combination of reference spectra to reproduce the XANES and EXAFS spectra from the sample was independently identified. The strategy was to use the minimum number of reference spectra to obtain a good fit of all sam-

Table A.7
Calculated contribution of upward diffusing Mn to the observed enrichment of total Mn at the sediment–water interface (0–0.5 cm) at station 7, 14 and 6.

Station (gradient (cm))	Upward diffusive porewater flux mmol m^{-2} yr^{-1}	Calculated surface enrichment μmol g^{-1}	Surface enrichment of total Mn μmol g^{-1}	Contribution of porewater Mn %
7 (0.25–1.75)	25.6	96	232	41
14(0.25–1.75)	14.6	55	574	9.6
6 (0.75–1.75)	7.7	29	229.8	12.6

The upward diffusive porewater flux (*mmol* m^{-2} yr^{-1}) was calculated using Eq. (A.7). The average porosity over these depth intervals was applied (i.e. 0.89 for all stations; Fig. A.8). The calculated enrichment is based on the upward diffusive flux and the sedimentation rate at the sediment–water interface. Upon a decrease in sedimentation rate, the role of upward diffusion of Fe(II) increases. Rates of sediment deposition at the shelf edge stations are low (Friedrich et al., 2002). The sedimentation rate at the open shelf is assumed to be 0.1 cm yr^{-1} (Wijsman et al., 2002). For this calculation we assumed an even lower rate of sedimentation of 0.01 cm yr^{-1}. The sediment enrichment (*mmol* g^{-1}) was calculated as follows,

$$\text{Sed.enrichment} = \text{upward diffusive flux}/(\text{sedimentation rate} * \text{sediment density} * 10^4) \quad (2)$$

The upward diffusive flux is expressed in units of μmol m^{-2} yr^{-1} and sedimentation rate in *cm* yr^{-1}. Sediment density was assumed to be 2.65 g cm^{-3} (Burdige, 2006). The contribution of the porewater flux is the percentage of the calculated surface enrichment based on upward diffusing dissolved Mn divided by the surface concentration of total Mn at 0–0.5 cm depth.

ple spectra. For this an R factor of less than 0.05 was taken as criterion for a sufficient good fit. Based on this procedure, at least three reference spectra were required. The optimum combination of reference spectra was the same for fitting the XANES and EXAFS spectra, which provides a more robust support for the interpretation of the spectra.

APPENDIX B. SUPPLEMENTARY MATERIAL

Supplementary data associated with this article can be found, in the online version, at https://doi.org/10.1016/j.gca.2020.01.031.

REFERENCES

Algeo T. J. and Tribovillard N. (2009) Environmental analysis of paleoceanographic systems based on molybdenum-uranium covariation. *Chem. Geol.* **268**(3–4), 211–225.

Aller R. C. (1994) Bioturbation and remineralization of sedimentary organic matter: effects of redox oscillation. *Chem. Geol.* **114** (3–4), 331–345.

Anderson T. F. and Raiswell R. (2004) Sources and mechanisms for the enrichment of highly reactive iron in euxinic Black Sea sediments. *Am. J. Sci.* **304**(3), 203–233.

Arthur M. A. and Dean W. E. (1998) Organic-matter production and preservation and evolution of anoxia in the Holocene Black Sea. *Paleoceanography* **13**(4), 395–411.

Balzer W. (1982) On the distribution of iron and manganese at the sediment/water interface: thermodynamic versus kinetic control. *Geochim. Cosmochim. Acta* **46**(7), 1153–1161.

Beck K. C., Reuter J. H. and Perdue E. M. (1974) Organic and inorganic geochemistry of some coastal plain rivers of the southeastern United States. *Geochim. Cosmochim. Acta* **38**(3), 341–364.

Berelson W., McManus J., Coale K., Johnson K., Burdige D., Kilgore T., Colodner D., Chavez F., Kudela R. and Boucher J. (2003) A time series of benthic flux measurements from Monterey Bay, CA. *Cont. Shelf Res.* **23**(5), 457–481.

Borsboom M., Bras W., Cerjak I., Detollenaere D., Glastra Van Loon D., Goedtkindt P., Konijnenburg M., Lassing P., Levine Y. K., Munneke B., Oversluizen M., Van Tol R. and Vlieg E. (1998) The Dutch-Belgian beamline at the ESRF. *J. Synchrotron Radiat.* **5**(3), 518–520.

Boudreau B. P. (1997) Diagenetic models and their implementation. Modelling transport and reactions in aquatic sediments, 505. Springer, New York, p. 436. Diagenetic models and their implementation. Modelling transport and reactions in aquatic sediments.

Brewer P. G. and Spencer D. W. (1974) Distribution of some trace elements in Black Sea and their flux between dissolved and particulate phases. *Am. Assoc. Pet. Geol. Bull. (United States)* **20**, 137–143.

Brown E. T., Le Callonnec L. and German C. R. (2000) Geochemical cycling of redox-sensitive metals in sediments from Lake Malawi: a diagnostic paleotracer for episodic changes in mixing depth. *Geochim. Cosmochim. Acta* **64**(20), 3514–3523.

Brumsack H. J. (2006) The trace metal content of recent organic carbon-rich sediments: implications for Cretaceous black shale formation. *Palaeogeogr. Palaeoclimatol. Palaeoecol.* **232**(2–4), 344–361.

Burdige D. J. (1993) The biogeochemistry of manganese and iron reduction in marine sediments. *Earth-Sci. Rev.* **35**(3), 249–284.

Burdige D. J. (2006) *Geochemistry of Marine Sediments*. Princeton University Press.

Burdige D. J. and Nealson K. H. (1986) Chemical and microbiological studies of sulfide mediated manganese reduction. *Geomicrobiol. J.* **4**(4), 361–387.

Calvert S. and Pedersen T. (1993) Geochemistry of recent oxic and anoxic marine sediments: implications for the geological record. *Mar. Geol.* **113**(1–2), 67–88.

Charette M. A., Lam P. J., Lohan M. C., Kwon E. Y., Hatje V., Jeandel C., Shiller A. M., Cutter G. A., Thomas A., Boyd P. W., Homoky W. B., Milne A., Thomas H., Andersson P. S., Porcelli D., Tanaka T., Geibert W., Dehairs F. and Garcia-Orellana J. (2016) Coastal ocean and shelf-sea biogeochemical cycling of trace elements and isotopes: lessons learned from GEOTRACES. *Philos. Trans. Roy. Soc.* **374**(2081), 20160076.

Claff S. R., Sullivan L. A., Burton E. D. and Bush R. T. (2010) A sequential extraction procedure for acid sulfate soils: partitioning of iron. *Geoderma* **155**(3–4), 224–230.

Coolen M. J. L., Saenz J. P., Giosan L., Trowbridge N. Y., Dimitrov P., Dimitrov D. and Eglinton T. I. (2009) DNA and lipid molecular stratigraphic records of haptophyte succession in the Black Sea during the Holocene. *Earth Planet. Sci. Lett.* **284**(3–4), 610–621.

Cutter G. A. and Kluckhohn R. S. (1999) The cycling of particulate carbon, nitrogen, sulfur, and sulfur species (iron monosulfide, greigite, pyrite, and organic sulfur) in the water columns of Framvaren Fjord and the Black Sea. *Mar. Chem.* **67**(3–4), 149–160.

De Baar H. J. W., Timmermans K. R., Laan P., De Porto H. H., Ober S., Blom J. J., Bakker M. C., Schilling J., Sarthou G., Smit M. G. and Klunder M. (2008) Titan: A new facility for ultraclean sampling of trace elements and isotopes in the deep oceans in the international Geotraces program. *Mar. Chem.* **111** (1–2), 4–21.

De Lange G. J., Thomson J., Reitz A., Slomp C. P., Speranza Principato M., Erba E. and Corselli C. (2008) Synchronous basin-wide formation and redox-controlled preservation of a Mediterranean sapropel. *Nat. Geosci.* **1**(9), 606.

Dellwig O., Leipe T., März C., Glockzin M., Pollehne F., Schnetger B., Yakushev E. V., Böttcher M. E. and Brumsack H. J. (2010) A new particulate Mn-Fe-P-shuttle at the redoxcline of anoxic basins. *Geochim. Cosmochim. Acta* **74**(24), 7100–7115.

DeMaster D. J. (1981) The supply and accumulation of silica in the marine environment. *Geochim. Cosmochim. Acta* **45**(10), 1715–1732.

Dijkstra N., Kraal P., Séguret M. J., Flores M. R., Gonzalez S., Rijkenberg M. J. and Slomp C. P. (2018) Phosphorus dynamics in and below the redoxcline in the Black Sea and implications for phosphorus burial. *Geochim. Cosmochim. Acta* **222**, 685–703.

Eckert S., Brumsack H. J., Severmann S., Schnetger B., März C. and Fröllje H. (2013) Establishment of euxinic conditions in the Holocene Black Sea. *Geology* **41**(4), 431–434.

Faulkner K. M., Stevens R. D. and Fridovich I. (1994) Characterization of Mn(III) complexes of linear and cyclic desferrioxamines as mimics of superoxide dismutase activity. *Arch. Biochem. Biophys.* **310**(2), 341–346.

Force E. R. and Cannon W. F. (1988) Depositional model for shallow-marine manganese deposits around black shale basins. *Econ. Geol.* **83**(1), 93–117.

Friedrich J., Dinkel C., Friedl G., Pimenov N., Wijsman J., Gomoiu M.-T., Cociasu A., Popa L. and Wehrli B. (2002) Benthic nutrient cycling and diagenetic pathways in the northwestern black sea. *Estuar. Coast. Shelf Sci.* **54**(3), 369–383.

Grasshoff K., Kremling K. and Ehrhardt M. (2009) *Methods of Seawater Analysis*. John Wiley & Sons.

Hermans M., Lenstra W. K., van Helmond N. A. G. M., Behrends T., Egger M., Séguret M. J. M., Gustafsson E., Gustafsson B. G. and Slomp C. P. (2019) Impact of natural re-oxygenation on the sediment dynamics of manganese, iron and phosphorus in a euxinic Baltic Sea basin. *Geochim. Cosmochim. Acta* **246**, 174–196.

Homoky W. B., Hembury D. J., Hepburn L. E., Mills R. a., Statham P. J., Fones G. R. and Palmer M. R. (2011) Iron and manganese diagenesis in deep sea volcanogenic sediments and the origins of pore water colloids. *Geochim. Cosmochim. Acta* **75**(17), 5032–5048.

Homoky W. B., Weber T., Berelson W. M., Conway T. M., Henderson G. M., van Hulten M., Jeandel C., Severmann S. and Tagliabue A. (2016) Quantifying trace element and isotope fluxes at the ocean sediment boundary: a review. *Philos. Trans. Roy. Soc. A: Math. Phys. Eng. Sci.* **374**(2081), 20160246.

Huerta-Diaz M. A. and Morse J. W. (1990) A quantitative method for determination of trace metal concentrations in sedimentary pyrite. *Mar. Chem.* **29**, 119–144.

Huerta-Diaz M. A. and Morse J. W. (1992) Pyritization of trace metals in anoxic marine sediments. *Geochim. Cosmochim. Acta* **56**(7), 2681–2702.

Jeandel C., van Der Loeff M. R., Lam P. J., Roy-Barman M., Sherrell R. M., Kretschmer S., German C. and Dehairs F. (2015) What did we learn about ocean particle dynamics in the GEOSECS JGOFS era? *Prog. Oceanogr.* **133**, 6–16.

Jilbert T. and Slomp C. P. (2013) Iron and manganese shuttles control the formation of authigenic phosphorus minerals in the euxinic basins of the Baltic Sea. *Geochim. Cosmochim. Acta* **107**, 155–169.

Jung H., Chadha T. S., Kim D., Biswas P. and Jun Y. S. (2017) Photochemically assisted fast abiotic oxidation of manganese and formation of δ-MnO2 nanosheets in nitrate solution. *Chem. Commun.* **53**(32), 4445–4448.

Jürgensen A., Widmeyer J. R., Gordon R. A., Bendell-Young L. I., Moore M. M. and Crozier E. D. (2004) The structure of the manganese oxide on the sheath of the bacterium Leptothrix discophora: an XAFS study. *Am. Mineral.* **89**(7), 1110–1118.

Kelly S. D., Hesterberg D., Ravel B., Ulery A. L. and Richard Drees L. (2008) Analysis of soils and minerals using X-ray absorption spectroscopy. *Meth. Soil Anal.* **5**, 387–464.

Klinkhammer G. and Hudson A. (1986) Dispersal patterns for hydrothermal plumes in the South Pacific using manganese as a tracer. *Earth Planet. Sci. Lett.* **79**, 241–249.

Koschinsky A. and Hein J. R. (2003) Uptake of elements from seawater by ferromanganese crusts: solid-phase associations and seawater speciation. *Mar. Geol.* **198**(3–4), 331–351.

Kraal P., Dijkstra N., Behrends T. and Slomp C. P. (2017) Phosphorus burial in sediments of the sulfidic deep Black Sea: key roles for adsorption by calcium carbonate and apatite authigenesis. *Geochim. Cosmochim. Acta* **204**, 140–158.

Kraal P., Yücel M. and Slomp C. P. (2019) Turbidite deposition and diagenesis in the southwestern Black Sea: implications for biogeochemical cycling in an anoxic basin. *Mar. Chem.* **209**, 48–61.

Krachler R., Krachler R. F., Wallner G., Hann S., Laux M., Cervantes Recalde M. F., Jirsa F., Neubauer E., von der Kammer F., Hofmann T. and Keppler B. K. (2015) River-derived humic substances as iron chelators in seawater. *Mar. Chem.* **174**, 85–93.

Lagerström M. E., Field M. P., Séguret M., Fischer L., Hann S. and Sherrell R. M. (2013) Automated on-line flow-injection ICP-MS determination of trace metals (Mn, Fe Co, Ni, Cu and Zn) in open ocean seawater: application to the GEOTRACES program. *Mar. Chem.* **155**, 71–80.

Landing W. M. and Lewis B. L. (1991) Thermodynamic modeling of trace metal speciation in the Black Sea. In *Black Sea Oceanography*. Springer, pp. 125–160.

Large R. R., Halpin J. A., Danyushevsky L. V., Maslennikov V. V., Bull S. W., Long J. A., Gregory D. D., Lounejeva E., Lyons T. W., Sack P. J., McGoldrick P. J. and Calver C. R. (2014) Trace element content of sedimentary pyrite as a new proxy for deep-time ocean-atmosphere evolution. *Earth Planet. Sci. Lett.* **389**, 209–220.

Learman D. R., Voelker B. M., Madden A. S. and Hansel C. M. (2013) Constraints on superoxide mediated formation of manganese oxides. *Front. Microbiol.* **4**, 1–11.

Learman D. R., Voelker B. M., Vazquez-Rodriguez A. I. and Hansel C. M. (2011) Formation of manganese oxides by bacterially generated superoxide. *Nat. Geosci.* **4**(2), 95–98.

Lenstra W. K., Hermans M., Séguret M. J. M., Witbaard R., Behrends T., Dijkstra N., van Helmond N., Kraal P., Laan P. and Rijkenberg M. J. A. (2019) The shelf-to-basin iron shuttle in the Black Sea revisited. *Chem. Geol.* **511**, 314–341.

Lenz C., Behrends T., Jilbert T., Silveira M. and Slomp C. P. (2014) Redox-dependent changes in manganese speciation in Baltic Sea sediments from the Holocene Thermal Maximum: an EXAFS, XANES and LA-ICP-MS study. *Chem. Geol.* **370**, 49–57.

Lenz C., Jilbert T., Conley D. J. and Slomp C. P. (2015) Hypoxia-driven variations in iron and manganese shuttling in the Baltic Sea over the past 8 kyr. *Geochem. Geophys. Geosyst.* **16**(10), 3754–3766.

Lenz C., Jilbert T., Conley D. J., Wolthers M. and Slomp C. P. (2015) Are recent changes in sediment manganese sequestration in the euxinic basins of the Baltic Sea linked to the expansion of hypoxia? *Biogeosciences* **12**(16), 4875–4894.

Lepland A. and Stevens R. L. (1998) Manganese authigenesis in the Landsort Deep. *Baltic Sea. Mar. Geol.* **151**(1–4), 1–25.

Lewis B. and Landing W. (1991) The biogeochemistry of manganese and iron in the Black Sea. Deep Sea Research Part A. *Oceanogr. Res. Pap.* **38**, S773–S803.

Little S. H., Vance D., Lyons T. W. and McManus J. (2015) Controls on trace metal authigenic enrichment in reducing sediments: insights from modern oxygen-deficient settings. *Am. J. Sci.* **315**(2), 77–119.

Luther G. W. (2010) The role of one- and two-electron transfer reactions in forming thermodynamically unstable intermediates as barriers in multi-electron redox reactions. *Aquat. Geochem.* **16**(3), 395–420.

Lyons T. W. (1997) Sulfur isotopic trends and pathways of iron sulfide formation in upper Holocene sediments of the anoxic Black Sea. *Geochim. Cosmochim. Acta* **61**(16), 3367–3382.

Lyons T. W. and Severmann S. (2006) A critical look at iron paleoredox proxies: new insights from modern euxinic marine basins. *Geochim. Cosmochim. Acta* **70**(23), 5698–5722.

Madison A. S., Tebo B. M., Mucci A., Sundby B. and Luther G. W. (2013) Abundant porewater Mn(III) is a major component of the sedimentary redox system. *Science* **341**(6148).

McManus J., Berelson W. M., Severmann S., Johnson K. S., Hammond D. E., Roy M. and Coale K. H. (2012) Benthic manganese fluxes along the Oregon-California continental shelf and slope. *Cont. Shelf Res.* **43**, 71–85.

Moore C. M., Mills M. M., Arrigo K. R., Berman-Frank I., Bopp L., Boyd P. W., Galbraith E. D., Geider R. J., Guieu C., Jaccard S. L., Jickells T. D., Roche J. L., Lenton T. M., Mahowald N. M., Mara nón E., Marinov I., Moore J. K., Nakatsuka T., Oschlies A., Saito M. a., Thingstad T. F., Tsuda A. and Ulloa O. (2013) Processes and patterns of oceanic nutrient limitation. *Nat. Geosci.* **6**(9), 701–710.

Muramoto J. A., Honjo S., Fry B., Hay B. J., Howarth R. W. and Cisne J. L. (1991) Sulfur, iron and organic carbon fluxes in the Black Sea: sulfur isotopic evidence for origin of sulfur fluxes. Deep Sea Research Part A. *Oceanogr. Res. Pap.* **38**, S1151–S1187.

Nealson K. H., Tebo B. M. and Rosson R. A. (1988) Occurrence and mechanisms of microbial oxidation of manganese. *Adv. Appl. Microbiol.* **33**, 279–318.

Nikitenko S., Beale A. M., Van Der Eerden A. M., Jacques S. D., Leynaud O., O'Brien M. G., Detollenaere D., Kaptein R., Weckhuysen B. M. and Bras W. (2008) Implementation of a combined SAXS/WAXS/QEXAFS set-up for time-resolved in situ experiments. *J. Synchrotron Radiat.* **15**(6), 632–640.

Oldham V. E., Miller M. T., Jensen L. T. and Luther G. W. (2017) Revisiting Mn and Fe removal in humic rich estuaries. *Geochim. Cosmochim. Acta* **209**, 267–283.

Oldham V. E., Mucci A., Tebo B. M. and Luther G. W. (2017) Soluble Mn(III)L complexes are abundant in oxygenated waters and stabilized by humic ligands. *Geochim. Cosmochim. Acta* **199**, 238–246.

Oldham V. E., Siebecker M. G., Jones M. R., Mucci A., Tebo B. M. and Luther G. W. (2019) The Speciation and Mobility of Mn and Fe in Estuarine Sediments. *Aquat. Geochem.* **25**(3), 1–24.

Panin N. and Jipa D. (2002) Danube river sediment input and its interaction with the North-western Black Sea. *Estuar. Coast. Shelf Sci.* **54**, 551–562.

Pilson M. E. Q. (2012) *An Introduction to the Chemistry of the Sea*. Cambridge University Press.

Popa A. (1993) Liquid and sediment inputs of the Danube river into the north-western Black Sea. *Transp. Carbon Nutr. Lakes Estuaries* **6**, 137–149.

Postma D. (1985) Concentration of Mn and separation from Fe in sediments-I. Kinetics and stoichiometry of the reaction between birnessite and dissolved Fe(II) at 10 degrees C. *Geochim. Cosmochim. Acta* **49**(4), 1023–1033.

Poulton S. W. and Canfield D. E. (2005) Development of a sequential extraction procedure for iron: Implications for iron partitioning in continentally derived particulates. *Chem. Geol.* **214**(3–4), 209–221.

Raiswell R. and Canfield D. E. (2012) The iron biogeochemical cycle past and present. *Geochem. Perspect.* **1**(1), 1–220.

Raiswell R., Vu H. P., Brinza L. and Benning L. G. (2010) The determination of labile Fe in ferrihydrite by ascorbic acid extraction: methodology, dissolution kinetics and loss of solubility with age and de-watering. *Chem. Geol.* **278**(1–2), 70–79.

Ravel B. and Newville M. (2005) ATHENA, ARTEMIS, HEPHAESTUS: data analysis for X-ray absorption spectroscopy using IFEFFIT. *J. Synchrotron Radiat.* **12**(4), 537–541.

Raven J. A. (1990) Predictions of Mn and Fe use efficiencies of phototrophic growth as a function of light availability for growth and of C assimilation pathway. *New Phytol.* **116**(1), 1–18.

Rijkenberg M. J. A., de Baar H. J. W., Bakker K., Gerringa L. J. A., Keijzer E., Laan M., Laan P., Middag R., Ober S., van Ooijen J., Ossebaar S., van Weerlee E. M. and Smit M. G. (2015) PRISTINE, a new high volume sampler for ultraclean sampling of trace metals and isotopes. *Mar. Chem.* **177**, 501–509.

Rijkenberg M. J. A., Middag R., Laan P., Gerringa L. J. A., Van Aken H. M., Schoemann V., De Jong J. T. M. and De Baar H. J. W. (2014) The distribution of dissolved iron in the West Atlantic Ocean. *PLoS ONE* **9**(6), 1–14.

Sander S. G. and Koschinsky A. (2011) Metal flux from hydrothermal vents increased by organic complexation. *Nat. Geosci.* **4**(3), 145–150.

Santelli C. M., Webb S. M., Dohnalkova A. C. and Hansel C. M. (2011) Diversity of Mn oxides produced by Mn (II)-oxidizing fungi. *Geochim. Cosmochim. Acta* **75**(10), 2762–2776.

Schlitzer R. (2015). Ocean Data View. 2012. Available: http://odv.awi.de.

Scholz F., McManus J. and Sommer S. (2013) The manganese and iron shuttle in a modern euxinic basin and implications for molybdenum cycling at euxinic ocean margins. *Chem. Geol.* **355**, 56–68.

Severmann S., McManus J., Berelson W. M. and Hammond D. E. (2010) The continental shelf benthic iron flux and its isotope composition. *Geochim. Cosmochim. Acta* **74**(14), 3984–4004.

Shaw T. J., Gieskes J. M. and Jahnke R. A. (1990) Early diagenesis in differing depositional environments: the response of transi-

tion metals in pore water. *Geochim. Cosmochim. Acta* **54**(5), 1233–1246.

Shiller A. M., Duan S., Van Erp P. and Bianchi T. S. (2006) Photo-oxidation of dissolved organic matter in river water and its effect on trace element speciation. *Limnol. Oceanogr.* **51**(4), 1716–1728.

Slomp C., Malschaert J., Lohse L. and Van Raaphorst W. (1997) Iron and manganese cycling in different sedimentary environments on the North Sea continental margin. *Cont. Shelf Res.* **17** (9), 1083–1117.

Soetaert K., Petzoldt T., and Meysman F. (2010). Marelac: Tools for aquatic sciences.

Spencer D. W. and Brewer P. G. (1971) Vertical advection diffusion and redox potentials as controls on the distribution of manganese and other trace metals Dissolved in waters of the Black Sea. *J. Geophys. Res.* **76**, 5877–5892.

Stoll M. H. C., Bakker K., Nobbe G. H. and Haese R. R. (2001) Continous-flow analysis of dissolved inorganic carbon content in seawater. *Anal. Chem.* **73**(17), 4111–4116.

Strickland J.D.H. and Parsons T.R. (1972). A practical handbook of seawater analysis. Fisheries Research Board of Canada.

Stumm W. and Morgan J. J. (1996) *Aquatic Chemistry: Chemical Equilibria and Rates in Natural Waters*. Wiley.

Suess E. (1979) Mineral phases formed in anoxic sediments by microbial decomposition of organic matter. *Geochim. Cosmochim. Acta* **43**(3), 352–399.

Sulu-Gambari F., Seitaj D., Behrends T., Banerjee D., Meysman F. J. R. and Slomp C. P. (2016) Impact of cable bacteria on sedimentary iron and manganese dynamics in a seasonally-hypoxic marine basin. *Geochim. Cosmochim. Acta* **192**, 49–69.

Sundby B., Anderson L. G., Hall P. O. J., Iverfeldt Å., van der Loeff M. M. R. and Westerlund S. F. G. (1986) The effect of oxygen on release and uptake of cobalt, manganese, iron and phosphate at the sediment-water interface. *Geochim. Cosmochim. Acta* **50**(6), 1281–1288.

Tankéré S. P. C., Muller F. L. L., Burton J. D., Statham P. J., Guieu C. and Martin J. M. (2001) Trace metal distributions in shelf waters of the northwestern Black Sea. *Cont. Shelf Res.* **21** (13–14), 1501–1532.

Tebo B. M. (1991) Manganese(II) oxidation in the suboxic zone of the Black Sea. *Deep Sea Res. Part A Oceanogr. Res. Pap.* **38**, 883–905.

Tebo B. M., Bargar J. R., Clement B. G., Dick G. J., Murray K. J., Parker D., Verity R. and Webb S. M. (2004) Biogenic manganese oxides: properties and mechanisms of formation. *Annu. Rev. Earth Planet. Sci.* **32**, 287–328.

Tebo B. M., Johnson H. A., McCarthy J. K. and Templeton A. S. (2005) Geomicrobiology of manganese(II) oxidation. *Trends Microbiol.* **13**(9), 421–428.

Thamdrup B., Glud R. N. and Hansen J. W. (1994) Manganese oxidation and in situ manganese fluxes from a coastal sediment. *Geochim. Cosmochim. Acta* **58**(11), 2563–2570.

Trouwborst R. E., Clement B. G., Tebo B. M., Glazer B. T. and Luther G. W. (2006) Soluble Mn(III) in suboxic zones. *Science* **313**(5795), 1955–1957.

van Hulten M. M. P., Middag R., Dutay J. C., de Baar H. J. W., Roy-Barman M., Gehlen M., Tagliabue A. and Sterl A. (2017) Manganese in the West Atlantic Ocean in context of the first global ocean circulation model of manganese. *Biogeosciences* **14**, 1123–1152.

Van Santvoort P. J., De Lange G. J., Thomson J., Colley S., Meysman F. J. and Slomp C. P. (2002) Oxidation and origin of organic matter in surficial Eastern Mediterranean hemipelagic sediments. *Aquat. Geochem.* **8**(3), 153–175.

Vieira L. H., Achterberg E. P., Scholten J., Beck A. J., Liebetrau V., Mills M. M. and Arrigo K. R. (2019) Benthic fluxes of trace metals in the Chukchi Sea and their transport into the Arctic Ocean. *Mar. Chem.* **208**, 43–55.

Von Langen P. J., Johnson K. S., Coale K. H. and Elrod V. A. (1997) Oxidation kinetics of manganese (II) in sea water at nanomolar concentrations. *Geochim. Cosmochim. Acta* **61**(23), 4945–4954.

Webb S. M., Tebo B. M. and Bargar J. R. (2005) Structural characterization of biogenic Mn oxides produced in seawater by the marine bacillus sp. strain SG-1. *Am. Mineral.* **90**, 1342–1357.

Wijsman J. W. M., Herman P. M. J. and Gomoiu M. T. (1999) Spatial distribution in sediment characteristics and benthic activity on the northwestern Black Sea shelf. *Mar. Ecol. Prog. Ser.* **181**, 25–39.

Wijsman J. W. M., Herman P. M. J., Middelburg J. J. and Soetaert K. (2002) A model for early diagenetic processes in sediments of the continental shelf of the black sea. *Estuar. Coast. Shelf Sci.* **54**, 403–421.

Wijsman J. W. M., Middelburg J. J. and Heip C. H. R. (2001) Reactive iron in black sea sediments: implications for iron cycling. *Mar. Geol.* **172**(3–4), 167–180.

Witbaard R., Duineveld G. C. A., Van der Weele J. A., Berghuis E. M. and Reyss J. P. (2000) The benthic response to the seasonal deposition of phytopigments at the Porcupine Abyssal Plain in the North East Atlantic. *J. Sea Res.* **43**(1), 15–31.

Yakushev E., Pakhomova S., Sørenson K. and Skei J. (2009) Importance of the different manganese species in the formation of water column redox zones: Observations and modeling. *Mar. Chem.* **117**(1–4), 59–70.

Associate editor: Caroline L. Peacock